European Journal of Medicinal Chemistry 46 (2011) 2043–2057

Contents lists available at ScienceDirect

European Journal of Medicinal Chemistry

journal homepage: http://www.elsevier.com/locate/ejmech

Original article

Discovery, synthesis, and investigation of the antitumor activity of novel piperazinylpyrimidine derivatives

Hassan M. Shallal, Wade A. Russu*

Department of Pharmaceutics & Medicinal Chemistry, Thomas J. Long School of Pharmacy and Health Sciences, University of the Pacific, 3601 Pacific Ave., Stockton, CA 95211, USA

ARTICLE INFO

Article history:
Received 22 November 2010
Received in revised form
19 February 2011
Accepted 22 February 2011
Available online 3 March 2011

Keywords:
Piperazinylpyrimidine
NCI-60
Kinases
MDA-MB-468

ABSTRACT

Protein kinases play several pertinent roles in cell proliferation, and targeting these proteins has been shown to be a successful strategy toward controlling different malignancies. Despite the great discovery stories during the last two decades, there is still a demand for anticancer small molecules with the potential of being selective on both the protein kinase and/or the cellular level. A series of novel piperazinylpyrimidine compounds were synthesized and tested for their potential to selectively inhibit the growth of certain tumor cell lines included within the NCI-60 cell line panel. MDA-MB-468, a triple-negative/basal-like breast carcinoma, cell line was among the most sensitive cell lines towards compounds **4** and **15**. The three most interesting compounds identified in cellular screens (**4**, **15**, and **16**) were subjected to kinase profiling and found to have an interesting selective tendency to target certain kinase subfamily members; PDGFR, CK1, RAF and others. Compound **4** showed a selective tendency to bind to and/or inhibit the function of certain KIT and PDGFRA mutants compared to their wild-type isoforms. Piperazinylpyrimidine based derivatives represent a new class of selective kinase inhibitors. Significantly **4** is more potent at inhibiting oncogenic mutant forms of PDGFR family kinases, which is relevant in terms of its potential use in treating tumors that have become resistant to treatment or driven by such mutations. The clinical demand for agents useful in the control of triple-negative/basal-like breast cancer justifies our interest in compound **15** which is a potent growth inhibitor of MDA-MB-468 cell line.

1. Introduction

The human kinome, represented by 518 kinases, is probably one of the most investigated protein families on biological, chemical, and clinical levels. This is mainly due to the fact that protein kinases are involved in the majority of signal transduction pathways regulating the cell machinery of survival, proliferation and maintenance. Accordingly, several pathological abnormalities are correlated with aberrations in the operational integrity and accuracy of certain kinases inside the cell. This makes kinases very attractive targets for treating, diagnosing and establishing personalized therapies of various disorders such as different malignancies, neurodegenerative disorders, rheumatoid arthritis, autoimmune diseases, and others [1–4]. Kinase inhibitors, either small molecules or monoclonal antibodies, represent a very strategic class of molecularly targeted anticancer agents; a statement that is easily verified by noting that approximately 14 kinase targeting agents have earned FDA approval during the last two decades as either anticancer or antiangiogenic agents. In comparison, not as many agents targeting other caner-relevant families such as Bcl-2 proteins, histone deacetylases, and phosphatases, have gained regulatory approval. Furthermore, the discovery, preclinical, and clinical development of novel kinase inhibitors currently absorb the lion's share of pharmaceutical industry developmental budgets and research efforts especially those who are seeking novel and effective cancer controlling agents [5,6].

As commonly believed by the kinase focusing research community, the design of selective kinase inhibitors has proven to be quite a challenging task due to the conservation of ATP-binding site, targeted by most inhibitors, among different kinases. Several design strategies, both computer assisted, bioinformatics aided, and structural based, have been implemented to tailor more selective kinase inhibitors against a subset of kinases or certain kinase subfamilies [2,7–13]. One successful example is lapatinib which is known to be a selective inhibitor against many wild-type

* Corresponding author. Tel.: +1 209 946 2339; fax: +1 209 946 2160.
E-mail address: wrussu@pacific.edu (W.A. Russu).

0223-5234/$ – see front matter © 2011 Elsevier Masson SAS. All rights reserved.
doi:10.1016/j.ejmech.2011.02.057

and mutant EGFR subfamily members and is currently utilized clinically in combination with capecitabine for metastatic breast cancer. In contrast, sunitinib, another successfully marketed kinase inhibitor, has been shown in several studies to be a highly promiscuous agent capable of interacting with more than 15% of kinases with a very high affinity ($K_d < 100$ nM) [14,15]. The selectivity of lapatinib compared to the promiscuity of sunitinib is usually rationalized by the observation that lapatinib is a type-II inhibitor which binds to the ATP-binding site as well as penetrating the adjacent allosteric binding site of its target kinases, whereas sunitinib is a type-I inhibitor that binds mainly to the ATP-binding site of several kinases [16,17]. However, it is unjustified, according to several published reports, to claim that every type-I kinase inhibitor is promiscuous and that every type-II inhibitor is selective [15,18]. Additionally, a given small molecule kinase inhibitor usually tends to recognize a given conformational ensemble of its target kinase(s) that may happen to differentially belong to either the active and/or the inactive state. That is to say that a type-I inhibitor, for example, may still bind to the inactive form of its kinase but with less affinity than with the active state. Considering another dimension of variability, some inhibitors interact potently with both the active and the inactive forms of their targeted kinases. For example, MK-2461 is able to bind with considerable potency to both the phosphorylated and the unphosphorylated forms of c-MET kinase with a measured binding constant (K_d) of 4.4 and 27.2 nM respectively [19]. Contrary to the behavior of MK-2461, sunitinib exhibits a strong differential selectivity towards the unactivated wild-type KIT versus the active form [16]. Generally speaking, the clinical fact that both lapatinib and sunitinib have successfully helped save or at least improve the life quality of certain cancer patient populations illustrates that, when it comes to kinase inhibitors, it is arguable that selectivity is always a virtue and non-selectivity is a constant drawback. In fact, some kinase modulating agents may achieve better clinical outcomes via targeting several kinases whereas others can cause troublesome side effects even while being selective [20]. Moreover, small molecules generally and kinase inhibitors specifically are usually promiscuous hitters of several protein families and that could explain why not all potent kinase inhibitors survive through the drug development process [21]. The phenomenon of kinase inhibitors being mostly non-selective has inspired the founding of several high-throughput kinase profiling screens in order to help determining intended as well as off-target kinases affected by a given kinase inhibitor [15,22,23]. These screens have made it possible to investigate the kinase binding potential or the functional inhibitory activity of a given small molecule against a large panel of kinases and thereby have facilitated uncovering some of the structural features relevant to promiscuity. Considering the current information we have about both kinases and their inhibitors, it is unreasonable to claim that a given small molecule is either selective or promiscuous kinase inhibitor without experimental support via performing a larger scale kinase profiling. However, it is now appreciated that the kinome space along with its multidimensional conformational space depends on structural features, at the primary, secondary and tertiary levels, that make a given kinase more promiscuous than another even with a difference of only a few amino acids [24]. Attention has been brought to the necessity of a deeper understanding of the promiscuity from the perspective of the protein kinases which has revealed very interesting correlations between the ATP-binding sites of certain subfamilies that are not closely related based on sequence similarity [25]. Resistance through several mechanisms, most frequently single point mutation, has been developed by cancer cells towards several kinase inhibitors; those that target proliferation and/or angiogenesis including both selective and non-selective kinase inhibitors [26–28].

The major aim of this report is to identify new lead molecules, from a series of novel piperazinylpyrimidine derivatives, which inhibit the growth of cancer cell lines. This series design is rationally based on targeting kinases. The kinase binding and inhibition activity of the most potent molecules is presented.

2. Results & discussion

2.1. Design

Our major aim was to investigate the potential of novel piperazinylpyrimidine derivatives to achieve antiproliferative activity and/or kinase binding. Piperazinylpyrimidine moiety was chosen because of its synthetic accessibility, availability of relevant starting materials, and its ability to provide four H-bond accepting nitrogens symmetrically oriented in space. In the current investigation, a systematic attachment of a quinazoline ring, recognized as a kinase privileged fragment, to the piperazinylpyrimidine moiety, through linkers that position the two aforementioned fragments in different relative orientations, has been adopted by our group as a strategy in our quest to discover novel anticancer agents and/or prototype kinase inhibitors. Towards achieving this goal, a novel series of 16 compounds, that are easily synthesized, were designed to target the human kinome via linking the two major fragments, mentioned above, either directly, group-I, or through an orientation linker, group-II, which offers more rigidity ($n = 0$) or more flexibility ($n = 1$) (Fig. 1). It is important to mention that only aromatic linkers based on benzene ring were chosen in this study to avoid excessive conformational flexibility inherent to aliphatic linkers and to facilitate deriving spatial-activity relationships. Additionally, considering that synthetic accessibility is one of the major factors that should be considered during the early design phase, starting materials allowing the incorporation of aromatic linkers are much more readily available and cheaper than their aliphatic analogs. The designed derivatives were tailored to localize to the hinge region of kinases via their kinase privileged fragment and extend either through the ATP-binding groove or towards the adjacent allosteric site so as to be either type-I or type-II inhibitors respectively or perhaps even adopt a novel binding mode. There are two major rationales upon which this design strategy is based i) certain kinases within the massive kinome space, 518 kinases adopting a wide range of conformational ensembles of both active and inactive states, may be able to accommodate the piperazinylpyrimidine scaffold attached directly or indirectly to the quinazoline moiety; the relevant question to be addressed is whether this is true or not and if it is true, which kinases are sensitive to these designed compounds, and ii) exploiting the steric space of a given class of small molecules with very similar chemical features that are positioned differently within the binding site may generate more than one lead kinase inhibitor with different respective

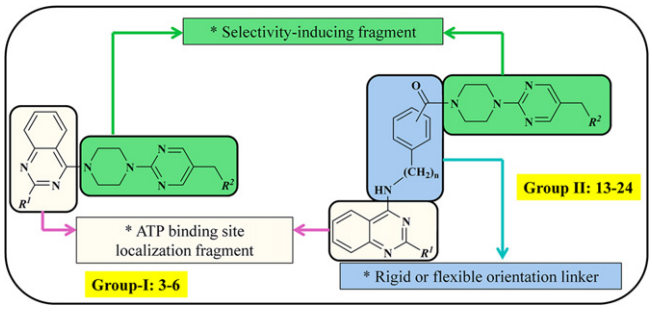

Fig. 1. Design strategy of final compounds **3**–**6** and **13**–**24**.

kinase selectivity profiles and/or anticancer cellular activity. We decided to narrow down the compounds to be kinome profiled by using anticancer cellular assays as primary screening followed by kinase profiling of only those compounds with encouraging cellular activity profiles and that incorporated different linkers. Such an order of experiments would avoid missing possible cytotoxic or cytostatic lead compounds which may fail to interact with their intended targets and happen to interact with another protein family that wasn't anticipated. This initial set of designed compounds was intended to be followed by a latter optimization cycle if they failed to show any promising activity on both the cellular and protein levels or to be further investigated if they exhibited interesting profiles on either the cellular or the protein level.

2.2. Chemistry

The final compounds were derived from two major piperazinylpyrimidine key intermediates (Schemes 1 and 2). The availability of starting materials made the execution of two different schemes for synthesizing two otherwise structurally similar intermediates convenient. Intermediate **1** was reported in the literature and the deprotection step was performed using HCl/MeOH method [29]. Intermediate **2** was synthesized using palladium catalyzed Suzuki cross coupling followed by deprotection as illustrated in Scheme 2. Group-1 compounds (**3**–**6**) were prepared directly by allowing the respective 4-chloroquinazoline derivative to react with one of the piperazinylpyrimidine intermediates (Scheme 3). Group-I compounds represent the direct attachment between the ATP-binding site localizing quinazoline fragment and the selectivity inducing piperazinylpyrimidine scaffold. Intermediates **7**–**12** were synthesized by allowing m-aminobenzoic acid, p-aminobenzoic acid, or p-aminomethylbenzoic acid to react with the corresponding quinazoline derivative using similar reaction conditions to those implemented in preparing group-I compounds (Scheme 4). Scheme 4 demonstrates the connection of the quinazoline fragment with the different linkers implemented in the design of group-II compounds (**13**–**24**). Group-II derivatives were prepared via coupling the carboxylic acid group of the intermediates (**7**–**12**) with the secondary aliphatic amine functionality of either intermediate **1** or intermediate **2** using EDC. HCl and triethylamine mixture as outlined in Scheme 5. Group-II is structurally different from group-I via the incorporation of a linker between the two major fragments. Such a linker strategy offers three different options; m-aminophenylcarbonyl and p-aminophenylcarbonyl provide similar rigidity level while orienting the fragments differently whereas p-aminomethylphenylcarbonyl provides more flexibility that allows the compound to cover more conformational space in orienting the major fragments.

2.3. In vitro cellular screening

Target compounds, **3**–**6** and **13**–**24**, were screened in-house against A549 (NSCLC) and MCF7 (breast cancer) cell lines to test the target compounds' cytotoxic potential and to reduce the number of compounds to be further investigated (data not shown). Structures of the active compounds were submitted for screening against the NCI-60 cell lines panel. Compounds (**3**–**4**, **13**, **15**–**16**, and **19**–**23**)

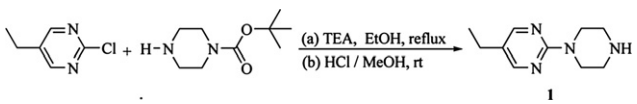

Scheme 1.

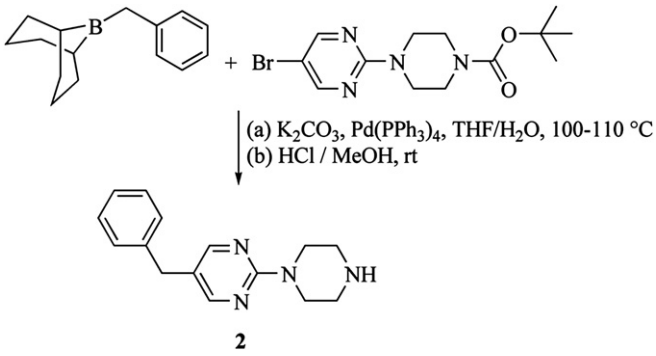

Scheme 2.

were initially accepted for screening against the NCI-60 at a single concentration of 10 μM. Eight out of the above compounds (**3**–**4**, **13**, **15**–**16**, and **19**–**21**) showed a significant antiproliferative activity at a 10 μM dose and were accordingly evaluated at five concentrations in order to determine their dose-response behavior and calculate their GI_{50} (dose inhibiting 50% of the growth compared to the control), TGI (dose inhibiting the growth completely), and LC_{50} (dose killing 50% of the starting cell population) values. Table 1 shows the GI_{50}, TGI, and LC_{50} values for compounds **4**, **15**, and **16**. Three compounds (**3**–**4** and **15**) showed an interesting pattern of selective cytotoxic activity and were submitted for retesting in order to confirm the reproducibility of their cellular actions. The three compounds gave reproducible results and compound **15** has been chosen by the DTP-BEC (Developmental Therapeutic Program-Biological Evaluation Committee) to advance to testing *in vivo* [30–32]. Compounds **3** and **4** gave very similar profile against the NCI-60 according to their structural similarity. However, **3** showed an overall partially weaker cytotoxic activity than **4** and that's why the former was neither considered in any further investigation nor will it be mentioned throughout the rest of the current report.

Compound **16** (NSC: D-750776) showed the highest overall potency and non-selectivity against the cell lines and it did not display a large difference between its cytostatic markers (mean GI_{50} = 1.05 μM and mean TGI = 3.24 μM) and cytotoxic indicator (LC_{50} = 22.91 μM). These data could be projected into potential toxicity against normal cells resulting in a narrow therapeutic index which may validate the decision made by the NCI-BEC not to advance **16** into animal testing. On the other hand, **4** (NSC: D-750901) and **15** (NSC: D-750905) displayed a very interesting pattern of selective cytostatic potency against certain cell lines scattered among tissues of different origin. For example, **15** was very potent against RPMI-8226 (leukemia, GI_{50} = 68 nM), NCI-H23 (lung, GI_{50} = 90 nM), SK-MEL-5 (skin, GI_{50} = 61 nM), and MDA-MB-468 (breast, GI_{50} = 30 nM) cancer cell lines. These two derivatives, **4** and **15**, also showed a remarkable difference between their cytostatic markers (mean GI_{50} & mean TGI) and cytotoxic indicator (mean LC_{50}). These data may classify **4** and **15** as cytostatic compounds whereas **16** may be described as a cytotoxic agent. According to the data presented in Table 1, and the testing reports

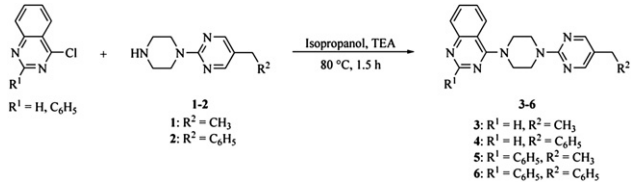

Scheme 3.

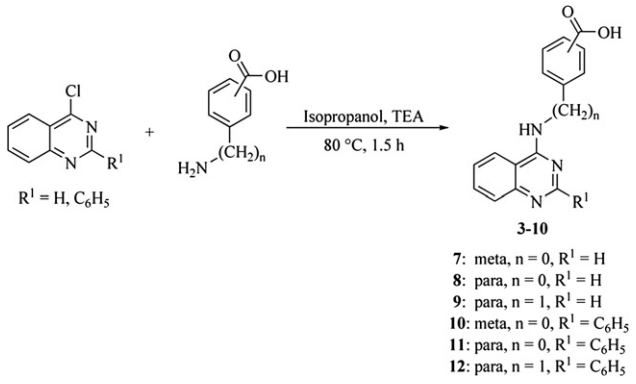

Scheme 4.

obtained from the NCI-60 screening, the relationships between the structure variations of the piperazinylpyrimidine derivatives and their cytostatic/cytotoxic activities can be summarized as shown in Fig. 2. A benzyl group in the 5-position of pyrimidine ring leads to more antiproliferative activity compared to ethyl substitution. Derivatives based on 2-phenylquinazoline show overall weaker antiproliferative potential compared to the unsubstituted quinazoline based derivatives. Concerning the linkers in group-II compounds, the para orientation shows the least cytotoxic activity whereas the meta positioning leads to the most potent derivatives with **16** being a clear example of this summation. Incorporation of a flexibility inducing element has refined the series into the very selective cytostatic performance of **15**. The strong correlation between the cellular profile of **4** (group-I) and **15** (group-II) in both terms of cellular selectivity and cytostatic rather than cytotoxic action raises the hypothesis that they both can affect similar set of targets in the cell and that **15**, through its flexible methylene group, is able to attain a conformational ensemble very similar to those attained by the more rigid derivative, **4**, devoid of a linker.

The concentration and time dependencies of the antiproliferative activity of compounds **4**, **15**, and **16** against MDA-MB-468 cell line were further investigated by our group using MTT assay. Several reasons have promoted us to give attention to this specific cell line. Firstly, this cell line represents the triple-negative/basal-like breast carcinoma which is more prevalent in younger women and women of African-American decent, is usually accompanied by frequent relapses and poor survival. As reported in the literature, there is a current therapeutic demand for efficient yet safe agents to be used in this specific clinical setting. Secondly, MDA-MB-468 cell line is significantly sensitive to DNA-damaging agents which are known to be highly toxic and non-selective [33].

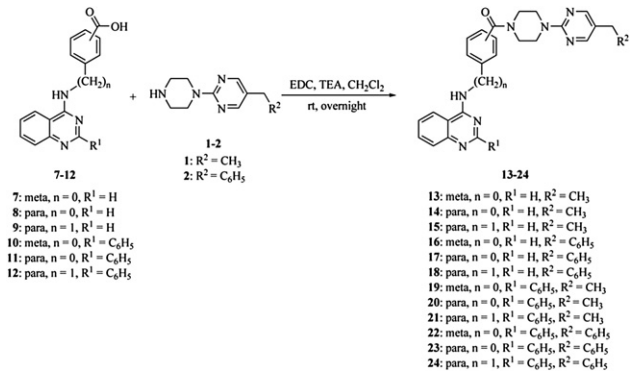

Scheme 5.

Therefore, the overall selectivity of compounds **4** and **15** against the NCI-60 cell line panel accompanied with their potent cytostatic action against MDA-MB-468 cell line represents an interesting phenomenon to be investigated. MDA-MB-468 cell line is known to overexpress EGFR receptor [34]. Therefore, gefitinib, known as an EGFR inhibitor, was included in the study as a positive control. According to the histogram shown in Fig. 3, the antiproliferative activity of a given test compound was directly proportional to the treatment time and the concentration. The ranking of activity according to the obtained IC_{50} values is as follows: **4** and **15** are both more antiproliferative than **16** than gefitinib against this specific cell line. A more in-depth biologically oriented investigation of the molecular mechanism of growth inhibitory action of **15** against MDA-MB-468 is currently ongoing and its results will be reported in due time.

From the above described *in vitro* cellular screening of several piperazinylpyrimidine derivatives, it can be concluded that some compounds belonging to this class exhibit different yet interesting behaviors against different cancer cell lines. This foundation prompted us to further investigate the promising derivatives and halt any further optimization effort for the meantime. **4**, **15**, and **16** were chosen for other experiments because they showed the most selective, **4** and **15**, or global, **16**, antitumor activity and because they represent the three major structural scenarios of this small class. At this point during the investigation, the question was whether these three compounds, shown to be optimized for promising cellular activity, are able to bind to kinases.

2.4. Kinase profiling of 4, 15, and 16

The presented series of novel compounds were structurally designed with the intention to interfere with certain members of the human kinome. Two major questions needed to be tackled. Firstly, can these compounds act as kinase inhibitors? And if they can, which kinases can they affect? Compounds **4**, **15**, and **16** were selected because they represent the three major structural determinants of our design and also because they were either selective cytostatic or potent cytotoxic on the cellular level. Compound **4** represents the direct attachment of the quinazoline ring with the piperazinylpyrimidine scaffold (group-I). Compound **15** exemplifies the use of a more flexible linker whereas compound **16** has a more rigid incorporated linker and both belong to group-II (Fig. 1). There are many commercial services established to facilitate screening against large panels of kinases. However, each method has its own benefits as well as limitations. Accordingly, two different kinase experiments were chosen for the current study. One is classified as a binding or non-biochemical assay while the other is functional and biochemically oriented [23].

In order to test the potential of **4**, **15**, and **16** to bind with the human kinome to which they were designed to target, a kinase binding assay was used to examine the ability of 10 μM of **4**, **15**, or **16** to interfere with the binding of a given kinase with an immobilized, ATP directed agent [15,35–40]. A single dose of 10 μM was chosen to allow for detecting kinases able to bind to the test compounds. In this binding assay, a set of 243 kinases were included. This set of kinases covers many possibilities i) wild-type versus mutant kinases ii) phosphorylated versus non-phosphorylated set of either wild-type or mutant ABL1 kinases (Table 2). For a complete list of the kinases tested, refer to the supporting information (Table S1). Details of the experiment are provided in the experimental section. It is however relevant to mention that a given interaction is represented by a numerical value called binding percentage of control (B-POC). The lower the B-POC value, the stronger the test compound binds with the test kinase. Only results with B-POC $\leq$ 50 are shown in Table 3. The kinases are ranked from

Table 1
The GI_{50} (dose inhibiting 50% of the growth compared to control), TGI (dose inhibiting the growth completely), and LC_{50} (Dose killing 50% of the starting number of cells) values result from screening of compounds **4**, **15**, and **16** against the NCI-60 cell line panel after 48 h treatment. All values are given in μM. Cells highlighted in cyan have GI_{50}values: $0 < GI_{50} \leq 0.1$ μM, while cells highlighted in yellow have values: $0.1 < GI_{50} \leq 1$ μM.

Tissue	Cell line	Compound **4**			Compound **15**			Compound **16**		
		GI_{50}	TGI	LC_{50}	GI_{50}	TGI	LC_{50}	GI_{50}	TGI	LC_{50}
Leukemia	CCRF-CEM	10.30	64.40	>100	10.00	60.90	>100	ND	ND	ND
	HL-6O(TB)	11.90	41.80	>100	11.20	38.60	>100	0.35	1.54	6.76
	K-562	0.47	>100	>100	0.37	>100	>100	0.37	2.23	>100
	M0LT-4	8.88	40.60	>100	4.02	27.60	>100	0.30	1.34	>100
	RPMI-8226	0.32	21.80	97.30	0.07	14.30	>100	0.21	0.60	3.89
Non-small cell lung cancer	A549/ATCC	7.82	35.70	>100	12.20	>100	>100	1.17	3.09	8.13
	EKVX	0.39	33.10	>100	0.20	61.40	>100	1.45	4.90	>100
	HOP-62	16.40	51.60	>100	18.20	>100	>100	1.62	3.47	7.41
	HOP-92	5.43	24.20	62.00	9.91	80.09	>100	ND	ND	>100
	NCI-H226	11.10	48.40	>100	5.96	>100	>100	0.42	2.09	7.94
	NCI-H23	0.44	30.80	>100	0.09	33.30	>100	1.07	2.69	6.92
	NCI-H322M	24.70	>100	>100	48.90	>100	>100	2.04	4.79	>100
	NCI-H460	10.20	23.70	55.00	5.06	30.70	>100	1.51	4.27	>100
	NCI-H522	13.80	40.30	>100	4.59	55.40	>100	0.62	2.09	5.13
Colon cancer	COLO 205	30.40	>100	>100	14.10	38.20	>100	1.41	2.75	5.50
	HCC-2998	15.90	60.90	>100	13.50	48.90	>100	1.78	3.98	8.91
	HCT-116	0.27	13.20	36.40	0.25	25.00	>100	1.07	3.55	>100
	HCT-15	19.40	63.20	>100	15.80	>100	>100	1.35	3.55	9.33
	HT29	15.50	35.10	79.20	14.00	83.20	>100	3.24	9.33	>100
	KM12	12.60	25.10	50.10	11.00	24.30	53.80	0.79	2.40	6.61
	SW-620	12.80	27.70	59.90	12.50	45.10	>100	1.91	4.27	>100
CNS cancer	SF-268	19.50	57.20	>100	27.50	>100	>100	2.57	>100	5.01
	SF-295	0.31	26.00	>100	0.22	23.10	>100	1.00	2.24	>100
	SF-539	14.40	28.50	56.10	36.40	>100	>100	1.95	4.90	>100
	SNB-19	12.30	>100	>100	11.00	>100	>100	2.82	8.91	>100
	SNB-75	16.50	78.20	>100	9.32	58.20	>100	2.34	5.89	>100
	U251	11.20	24.60	54.10	9.49	>100	>100	2.04	6.61	>100
Melanoma	LOX IMVI	0.86	19.60	44.30	0.53	28.70	97.30	1.15	2.45	5.13
	MALME-3M	12.70	33.60	89.20	6.25	42.20	>100	1.26	2.57	5.25
	M14	13.40	26.30	51.60	11.40	32.70	93.70	1.00	2.14	4.68
	MDA-MB-435	2.64	27.50	91.40	1.78	>100	>100	0.95	2.14	4.57
	SK-MEL-2	18.20	35.80	70.30	24.20	>100	>100	1.26	2.69	5.89
	SK-MEL-28	22.00	99.30	>100	22.70	>100	>100	1.48	2.82	5.25
	SK-MEL-5	0.15	13.90	37.70	0.06	2.90	20.80	0.31	1.20	3.47
	UACC-257	0.50	16.80	41.40	1.97	26.80	>100	1.29	2.63	5.37
	UACC-62	10.60	25.90	63.10	8.86	80.90	>100	0.48	1.86	5.37
Ovarian cancer	IGROVI	19.80	63.30	>100	16.70	49.80	>100	0.52	1.82	5.01
	OVCAR-3	11.20	23.20	48.20	15.40	>100	>100	1.62	8.13	>100
	OVCAR-4	0.09	>100	>100	0.16	58.80	>100	0.43	1.95	7.59
	OVCAR-5	19.40	69.80	>100	29.50	>100	>100	2.34	5.75	>100
	OVCAR-8	5.90	25.60	71.30	9.16	>100	>100	0.40	3.31	>100
	NCI/ADR-RES	0.63	17.60	66.40	0.68	21.50	>100	0.28	8.51	>100
	SK-OV-3	25.50	>100	>100	63.80	>100	>100	1.82	4.47	>100
Renal cancer	786–0	12.80	36.70	>100	10.70	54.80	>100	2.34	6.61	>100
	A498	11.70	24.20	50.10	37.50	>100	>100	0.63	5.37	>100
	ACHN	12.00	42.40	>100	3.61	82.50	>100	1.58	4.57	>100
	CAKI-1	3.79	39.30	>100	5.44	94.80	>100	0.59	1.91	4.47
	RXF 393	17.20	57.90	>100	14.30	41.60	>100	2.88	11.48	>100
	SN12C	10.90	24.40	54.80	7.24	59.00	>100	2.29	7.08	>100
	TK-10	13.70	60.80	>100	10.90	>100	>100	2.45	6.17	39.81
	UO-31	13.30	38.40	>100	4.90	60.50	>100	0.43	1.82	4.37
Prostate cancer	PC-3	15.60	>100	>100	10.50	>100	>100	0.66	2.88	>100
	DU-145	11.80	30.70	79.80	16.00	>100	>100	2.24	6.46	>100
Breast cancer	MCF7	3.24	58.20	>100	1.94	72.80	>100	0.85	2.29	5.62
	MDA-MB-231/ATCC	15.60	38.10	92.80	17.00	84.90	>100	2.45	2.95	>100
	HS 578T	20.00	54.80	>100	49.60	>100	>100	2.45	7.41	>100
	BT-549	1.26	18.40	43.00	0.34	10.70	>100	0.44	1.74	5.37
	T-47D	0.71	45.50	>100	1.25	>100	>100	0.24	7.59	5.62
	MDA-MB-468	0.06	2.73	>100	0.03	2.22	>100	0.74	3.47	>100
Mean		**5.24**	**37.15**	**81.28**	**4.46**	**51.28**	**>100**	**1.05**	**3.24**	**22.91**

the most to the least sensitive kinase towards binding with a given test compound. Table 3 illustrates that within the set of tested kinases, certain members of CDK, CK1, PDGFR, DDR, ABL, p38, RAF, or RIPK subfamilies were more or less recognized by the three test compounds. Some members of CK1 subfamily were commonly recognized by the three test compounds. 10 μM of compound **15** showed almost equal affinity to bind to several members of CK1 subfamily whereas CSNK1D was almost equivalently sensitive to the three derivatives; B-POC = 26 against **4**, B-POC = 23 against **15**, and B-POC = 22 against **16**. Another CKI member, CSNK1E, was found to be sensitive towards **15** and **16** more than towards **4**. CSNKIE has been found to be significantly expressed in several cancer types compared to their normal tissues [41]. The above results lead to the hypothesis that concerning CK1 subfamily members, the combination of piperazinylpyrimidine scaffold with quinazoline ring may be relevant for binding irrespective to the

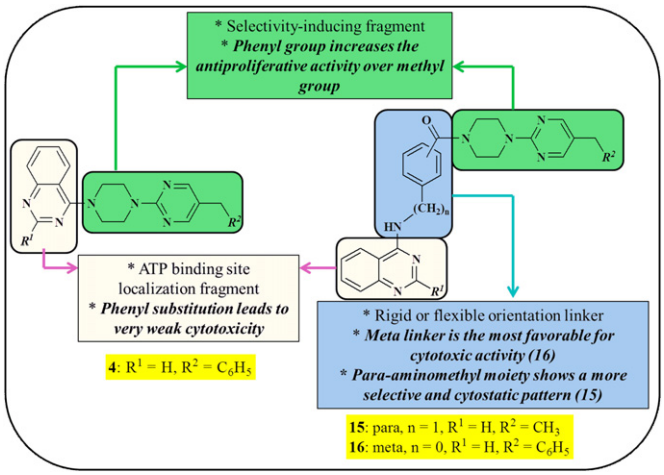

Fig. 2. The overall structure-antiproliferative activity relationships of piperazinylpyrimidines.

presence of linkers or a specific linker. The above observation suggests for CK1 family kinases, especially CSNK1D, there exists a common binding site which is able to accommodate piperazinylpyrimidine derivatives of different molecular sizes and linkers. In retrospect, the three test compounds have some structural similarities with purine derivatives found to be dual CDK/CK1 inhibitors [42]. Compound **4** exhibited obvious tendency to bind strongly with certain wild-type and/or mutant members of the CDK and PDGFR subfamilies. This could be attributed to a steric factor based on that **4** is smaller in size than both **15** and 1**6** and that the targeted binding site of these subfamilies, CDK and PDGFR, is unable to accommodate these larger derivatives (**15** and 1**6**). It is interesting to observe that **15** bound with higher affinity to BRAF and its common V600E mutant whereas **4** and **16** were recognized by RIPKI, another TKL (tyrosine kinase like) kinase. Among the tested unphosphorylated and phosphorylated derivatives of ABL1, only two close mutants were bound by the test compounds. ABL1(F317I) was moderately recognized by **4** (B-POC = 30) and **16** (B-POC = 20) whereas ABL1(F317L) was more strongly recognized by **15** (B-POC = 6.8). Since phosphorylated kinases are presumed to exist preferentially in the active state, the last observation raises the possibility of the ability of the test compounds to interact with active kinases and inhibit their phosphotransferase function.

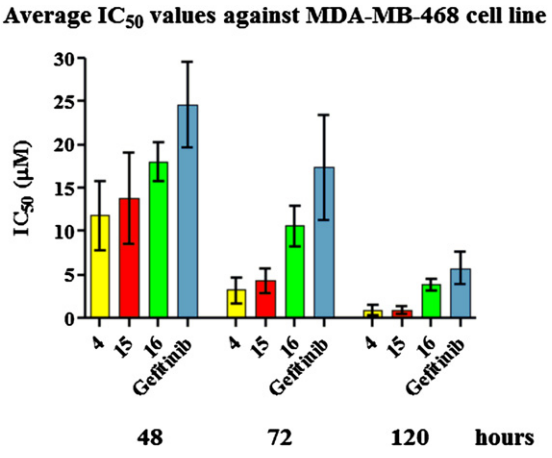

Fig. 3. The results of the MTT assay in which **4**, **15**, **16**, and gefitinib were screened against MDA-MB-468 cell line. The Histogram shows the average IC_{50} values in μM. The IC_{50} values were calculated using non-linear regression analysis as described in the experimental section. The error bars represent the 95% confidence interval calculated for 9n (three independent experiments, each is a triplicate).

Table 2
The phosphorylation status of kinases used in the single-dose kinase binding assay.

	Phosphorylated	Non-phosphorylated
Wild-type	1	198
Mutants	8	36

Accordingly, a biochemical functional screening of the test compounds was decided to be pursued within the current investigation. In terms of lead kinase subfamilies, it is interesting that **4** was able to target PDGFR wild-type and mutants without affecting ABL1 or ABL2 kinases (only phosphorylated ABL1(F317I) mutant was targeted by **4**). It is very common for inhibitors binding ABL subfamily to also target PDGFR subfamily and vice versa with Imatinib being a prime example of such behavior [43,44]. Compound **4** represents a prototype structure that can discriminate between PDFGR and ABL subfamilies. The test compounds, as prototype kinase binders, have excellent overall selectivity towards certain kinase subfamilies. Although **4** lacks the anilino NH group which is known to be one of the fundamental structural features of many kinase inhibitors, it shows clear potential to bind to certain kinases which supports the hypothesis that it is hard to have a common set of rules when designing kinase inhibitors [12]. Based on the results of this primary single-dose screen, we investigated the concentration-dependent potential of compound **4** to bind to FLT3, KIT, KIT(D816H), or KIT(D816V). This was achieved via determining the K_d (dissociation constant) of the four interactions (Table 3). The dose-response curves of compound **4** against FLT3, KIT, KIT(D816H), or KIT(D816V) are included in the supporting information (Fig. S2). The ability of **4** to differentially discriminate between certain KIT and FLT3 wild-type and mutant isoforms will be discussed latter.

In order to evaluate whether the molecules could inhibit the phosphotransferase kinase function, a radiometric based assay was used to measure the ability of 1 μM of compounds **4**, **15**, or **16** to

Table 3
The results of the kinase binding assay. The B-POC values of 10 μM of compounds **4**, **15**, and **16** against the most sensitive kinases tested within this binding experiment are given in the table (B-POC ≤ 50). Both the B-POC and K_d values are the average of duplicate measurements. ND indicates not determined.

Kinase	**Cmpd-4**		**Cmpd-15**	**Cmpd-16**
	B-POC	K_d (μM)	B-POC	B-POC
ABL1(F317I)-phosphorylated	30	ND	>50	20
ABL1(F317L)-phosphorylated	>50	ND	6.8	>50
BRAF	>50	ND	34	>50
BRAF(V600E)	>50	ND	13	>50
CDK8	3.4	ND	>50	>50
CDK11	0	ND	47	>50
CSF1R	31	ND	>50	>50
CSNK1A1	>50	ND	36	>50
CSNK1D	26	ND	23	22
CSNK1E	45	ND	29	23
CSNK1G2	>50	ND	18	43
CSNK1G3	>50	ND	24	>50
DDR1	47	ND	>50	28
FLT3	8.4	0.53	>50	>50
FLT3(D835H)	46	ND	>50	>50
FLT3(ITD)	49	ND	>50	>50
FLT3(K663Q)	4	ND	>50	>50
KIT	9.1	2.5	>50	>50
KIT(D816H)	30	1.3	>50	>50
KIT(D816V)	0.5	0.11	>50	>50
KIT(L576P)	9.8	ND	>50	>50
KIT(V559D)	4.3	ND	>50	>50
p38-gamma	>50	ND	>50	25
PDGFRA	21	ND	>50	>50
PDGFRB	4.1	ND	>50	>50
RIPK1	3.5	ND	>50	19

interfere with the function of a set of 55 protein kinases; 39 wild-type and 16 mutants (Table S2) [45,46]. This set of tested kinases was chosen based on the results of the binding assay described above. Again the ability of 1 μM of a given test compound to inhibit the phosphotransferase function of a given kinase is expressed by functional percentage of control (F-POC) value which is also inversely proportional to the potency of the test compound, at that specific concentration, for a given kinase. The most promising interactions, at a single dose, were further investigated to determine the IC_{50} values (Table 4). The IC_{50} of compound **4** was determined against KIT, KIT(D816H), KIT(D816V), KIT(V560G), FLT3, PDGFRA(V561D), and PDGFRA(D842V) (Table 4). Doses-response curves were used to determine the IC_{50} values (Fig. S3). The three test compounds, once again, weakly inhibited the same member of CK1 subfamily, CSNK1D. Compound **4** demonstrated the ability to inhibit the function of some PDGFR subfamily members; both wild-type and mutants, without affecting ABL subfamily members. On the other hand, 1**5** and **16** showed weak inhibitory action against ABL kinase and some members of PDGFR subfamily.

Both kinase profiling experiments, binding and functional, revealed a very interesting pattern by which compound **4** shows more potential to either bind to or inhibit the function of some of the KIT and PDGFRA mutants compared to their wild-type isoforms. Table 5 can be used to illustrate this phenomenon and aid in its analysis. The location of each mutation within the kinase different domains is included [16,47]. It has been reported that different gain-of-function mutations of the KIT kinase lead to constitutive catalytic activity independent of activation by extracellular stem cell factor. The occurrence of these mutations was detected in cases where marketed KIT inhibitors (imatinib, dasatinib and sunitinib) face resistance by the target cancer cells and become inefficacious in the treatment of chronic myeloid leukemia (CML) and/or gastrointestinal stromal tumors (GIST) [16,48,49]. Compound **4** showed higher activity against the KIT A-loop mutants; D816H and D816V compared to its activity against wild-type KIT, a foundation that is supported by both the K_d values in the binding screen and the IC_{50} values in the functional assay. As common with many other kinase inhibitors, mutations of the gatekeeper residue of KIT could render the protein less liable to binding by **4**; an observation reinforced by the significant increase in the B-POC value of the juxtamembrane mutant KIT(V559D) upon mutation of the gatekeeper in the double mutant KIT(V559D, T670I). This shows that the gatekeeper residue and probably the adjacent hinge region are critical in binding of **4** to KIT. It is clear that **4** was able to bind the KIT(D816V) ($K_d = 0.11$ μM) more than KIT(D816H) ($K_d = 1.3$ μM) whereas it inhibited the function of KIT(D816H) ($IC_{50} = 0.316$ μM) more than KIT(D816V) ($IC_{50} = 2.82$ μM). Such opposite effects, on two different mutations at the same location, could originate from the difference in the preferred conformational ensembles and highlights the potential effect of a single amino acid mutation upon the probability distribution of the protein's conformations to be selected for binding by a given small molecule like **4**. The ability of **4** to efficiently bind to certain KIT mutants, that are resistant to other kinase inhibitors, more than it binds to the wild-type isoform makes it valuable as a structural prototype and adds another virtue to its global selective kinase profile. Accordingly, **4** can be selective towards cancer phenotypes harboring and depending on such mutant KIT forms versus normal cells depending mainly on wild-type KIT to function. Compound **4** also exhibited a similar fashion of selectivity towards certain PDGFRA mutants (V561D in the juxtamembrane or D842V in the A-loop) as illustrated by the F-POC and IC_{50} determination. Such PDGFRA mutants exhibit differential resistance towards certain kinase inhibitors like imatinib and nilotinib and become common in certain forms of resistant cancer phenotypes [47,50–52].

Table 4
The results of the kinase function inhibition assay. The F-POC of 1 μM of compounds **4**, **15**, and **16** against selected kinases tested within this experiment. Both the F-POC and IC_{50} values are the average of duplicate measurement. ND indicates not determined.

Kinase	**Cmpd-4**		**Cmpd-15**	**Cmpd-16**
	F-POC	IC_{50} (μM)	F-POC	F-POC
ABL	92	ND	80	87
CSNK1D	90	ND	87	74
FLT3	74	6.692	80	95
KIT	94	>10.0	100	100
KIT(D816H)	30	0.316	100	100
KIT(D816V)	83	2.823	100	100
KIT(V560G)	36	0.699	99	86
MAPK1	100	ND	100	73
MET	75	ND	100	100
PDGFRA(D842V)	25	0.316	100	96
PDGFRA(V561D)	20	0.295	100	100
PKBβ	89	ND	82	83

Table 5
The potential of compound **4** to either bind to or inhibit the function of certain KIT or PDGFRA isoforms. The B-POC of 10 μM and F-POC of 1 μM of compound **4** measured in the binding and function inhibition experiments respectively. JM denotes for juxtamembrane domain, and GK denotes gatekeeper residue. ND indicates not determined.

Kinase	Location	B-POC	K_d (μM)	F-POC	IC_{50} (μM)
KIT(D816V)	A-loop	0.5	0.11	83	2.82
KIT(D816H)	A-loop	30	1.3	30	0.316
KIT(A829P)	A-loop	84	ND	ND	ND
KIT(V559D)	JM	4.3	ND	ND	ND
KIT(L576P)	JM	9.8	ND	ND	ND
KIT(V559D,T670I)	JM and GK	66	ND	ND	ND
KIT(V560G)	JM	ND	ND	36	0.699
KIT	Wild-type	9.1	2.5	94	>10.0
PDGFRA(V561D)	JM	ND	ND	20	0.295
PDGFRA(D842V)	A-loop	ND	ND	25	0.316
PDGFRA	Wild-type	21	ND	116	ND

Compound **15** demonstrated a similar trend of selectivity towards the mutant BRAF(V600E) versus the wild-type BRAF (Table 3). BRAF(V600E) mutant is commonly found in several kinds of cancer especially melanoma and GIST. This mutation has attracted the attention of research groups to develop specific inhibitors against it [50,53]. ABL1 mutants have been generally shown to affect the sensitivity towards ABL kinase inhibitors. Point mutations in codon 317 of ABL1 have been found to specifically impart resistance towards dasatinib [54–56]. Compound **4** and **16** have moderate affinity for the phosphorylated form of ABL1(F317I) while **15** has stronger binding affinity towards the phosphorylated form of ABL1(F317L). This observation again highlights the value of these test compounds' potential to be discretely selective towards certain kinase mutants.

As revealed by Table 3 and Table 4, although compounds **4** and **15** have certain common kinase targets, they don't share an overall similar selectivity profile in that **4** is more active towards the PDGFR subfamily. This is contrary to the striking correlation of their cellular profiles against the NCI-60 panel. It could be the case that **4** and **15**, very similarly, affect other kinases that are not included in the kinase profiling experiments reported here. Another possible scenario is that **4** and **15** could equally inhibit other protein(s) that belong to a different protein family other than protein kinases. It also may be possible that **4** and **15** target the same signaling transduction pathway at different points. The biological investigation of other possible targets is beyond the scope of the current report and we leave it for future studies that can investigate the global genomic and/or proteomic differences induced by **4** and **15** on the cellular level.

A question emerged at this level of investigation; how does **4** bind to its kinase targets generally and to wild-type and mutant

KIT versions specifically? To tackle this question, we compared the observed binding affinity of **4** against the wild-type KIT and its D816V mutant, obtained from the binding data, to the respective binding affinity of 38 kinase inhibitors against the same two kinases observed under very similar experimental conditions (Table 6) [15]. ΔΔG°, as a measure of the differential binding potential against the mutant KIT(D816V) versus the wild-type KIT, was calculated according to the literature [57,58]. A negative ΔΔG° indicates preferential binding to the mutant whereas a positive ΔΔG° indicates increased resistance by the mutant against the specific inhibitor. Analysis of Table 6 revealed a very interesting feature; the seven reference kinase inhibitors, that have negative ΔΔG°, are known to be type-I kinase inhibitors which bind to the same binding site occupied by ATP [22,59–64]. The above observation agrees with several published computational as well as experimental reports demonstrating that an aspartic acid to valine mutation in the position 816 of KIT destabilizes the inactive (DFG-out) conformations of KIT. The same mutation would consequently decrease the binding to type-II kinase inhibitors which mainly bind preferentially to the inactive (DFG-out) conformational ensemble of KIT [16,65,66]. The above notation coupled with the experimental tendency of **4** to bind better to the V816KIT compared to the D816KIT supports the hypothesis that **4** may be a type-I kinase inhibitor that targets the ATP-binding site in contrast to type-II inhibitors which exploit the adjacent allosteric binding site.

Table 6
Comparison of the behavior of **4** towards KIT and its mutant KIT(D816V) with a set of 38 structurally diverse kinase inhibitors. The K_d values of the reference kinase inhibitors were determined experimentally against the two kinases similarly to that of **4** and were obtained from literature [15]. ΔΔG° (Kcal.mol^{-1}) = R.T.ln [K_d(mutant)/K_d(wild-type)] where $R = 0.001985$ kcal mol^{-1} K^{-1} and $T = 298$ K.

Kinase inhibitor	Kd (nM)		ΔΔG°
	KIT	KIT(D816V)	
Staurosporine	19	0.64	−2.01
PKC-412	220	7.7	−1.98
4	2500	110	−1.847
LY-333531	>10,000	920	<−1.4
Erlotinib	>10,000	1600	<−1.08
Gefitinib	>10,000	4300	<−0.49
Flavopiridol	>10,000	4600	<−0.45
CI-1033	7800	3900	−0.41
ZD-6474	260	290	0.06
VX-680	240	290	0.11
JNJ-7706621	1800	2500	0.19
Dasatinib	0.62	2.6	0.85
Sorafenib	31	310	1.36
MLN-518	2.7	29	1.4
CHIR-265	200	6200	2.03
ABT-869	2	81	2.19
Imatinib	14	820	2.41
BIRB-796	170	>10,000	>2.41
AST-487	5.4	360	2.48
AMG-706	3.7	410	2.78
GW-786034	2.8	500	3.07
CHIR-258	7.5	1400	3.09
AZD-1152HQPA	17	4600	3.31
SU-14813	0.68	340	3.68
Sunitinib	0.37	380	4.1
PTK-787	5.1	>10,000	>4.48
BMS-387032	>10,000	>10,000	–
CP-690550	>10,000	>10,000	–
CP-724714	>10,000	>10,000	–
EKB-569	>10,000	>10,000	–
GW-2580	>10,000	>10,000	–
Lapatinib	>10,000	>10,000	–
MLN-8054	>10,000	>10,000	–
PI-103	>10,000	>10,000	–
Roscovitine	>10,000	>10,000	–
SB-202190	>10,000	>10,000	–
SB-203580	>10,000	>10,000	–
SB-431542	>10,000	>10,000	–
VX-745	>10,000	>10,000	–

2.5. Molecular docking

In order to visualize and generate a binding hypothesis of **4**, **15**, and 1**6** to their candidate kinases, a rigid docking experiment was performed where the mode of binding of those compounds to CSNK1D was simulated using Autodock 4 software [67]. The results of the static simulation show that **4**, **15**, or **16** can bind to CSNK1D as classical type-I inhibitors which usually occupies the ATP-binding site surrounded by the hinge region, P-loop, β6 strand and β9 strand [68]. None of the docked ligands exploited the allosteric binding site commonly occupied by type-II inhibitors [18]. CSNK1D was selected for the described docking session because it is equally capable of binding to 10 μM of any of the tested compounds according to the kinase binding experiment (Table 3).It is important to mention that the grid box was designed to be large enough to allow the software to choose between different modes of binding; type-I or type-II. Not only the interaction pattern predicted by this docking experiment agrees with our primary rationale of using the quinazoline ring as a hinge region localizing fragment, but also it supports the earlier mentioned hypothesis that **4** binds with KIT kinase as a typical type-I inhibitor. A clear steric complementarity between the available space in the ATP-binding site of CSNK1D and the size of the tested derivatives can be easily confirmed by the results of the above rigid docking (Fig. 4). Concerning the electrostatic complementarity, as commonly observed in the binding of type-I quinazoline based kinase inhibitors, a hydrogen bonding interaction was predicted, by the docking experiment, between the quinazoline nitrogen of a given ligand (**4**, **15** or **16**) as a hydrogen bond acceptor and the backbone NH of LEU88 residue in the hinge region as a hydrogen bond donor. Another H-bond was suggested between the carbonyl oxygen of **15** (acceptor) and the NH backbone of SER20 (donor) lies in the P-loop. Fig. 4 also shows the likelihood of a π-cation interaction between the pyrimidine ring of either **15** or **16** and the protonated LYS133 side chain located in the β6 strand. It can be easily speculated that under more realistic dynamic conditions of interaction, the last mentioned interaction could be a mix between π-cation interaction and H-bonding between one of the symmetric pyrimidine ring nitrogens in the bigger ligands (**15** or **16**) and the side chain quaternary amino group of LYS133. Accordingly, piperazinylpyrimidine can be hypothesized to interact with their respective kinase candidates as type-I inhibitors, a hypothesis that still needs experimental investigation using either x-ray crystallography or NMR spectroscopy.

2.6. Summary

In summary a primary lead discovery investigation identified **4**, **15**, and **16** to be highly optimized for selective cytostatic, as in the cases of **4** and **15**, or global cytotoxic activity, as in the case of **16**, against the NCI-60 panel. Consequently, **15** grabbed the attention of the NCI and is currently being investigated in animal models of cancer. Also noted is the very interesting phenomenon of **4** and **15** exhibiting reproducible selective cytostatic activity against MDA-MB-468 breast cancer cell line which represents a model for a clinically distinctive group of triple negative/basal-like breast cancer patients. This interesting selective antiproliferative activity against MDA-MB-468 cell line is concentration and time dependent and its mechanism at the molecular pathways level is currently being investigated. Kinase profiling experiments were chosen to detect the ability of **4**, **15**, and **16** to either bind to or inhibit the function of a large panel of kinases. Both kinase binding and function inhibition experiments showed an overall selective

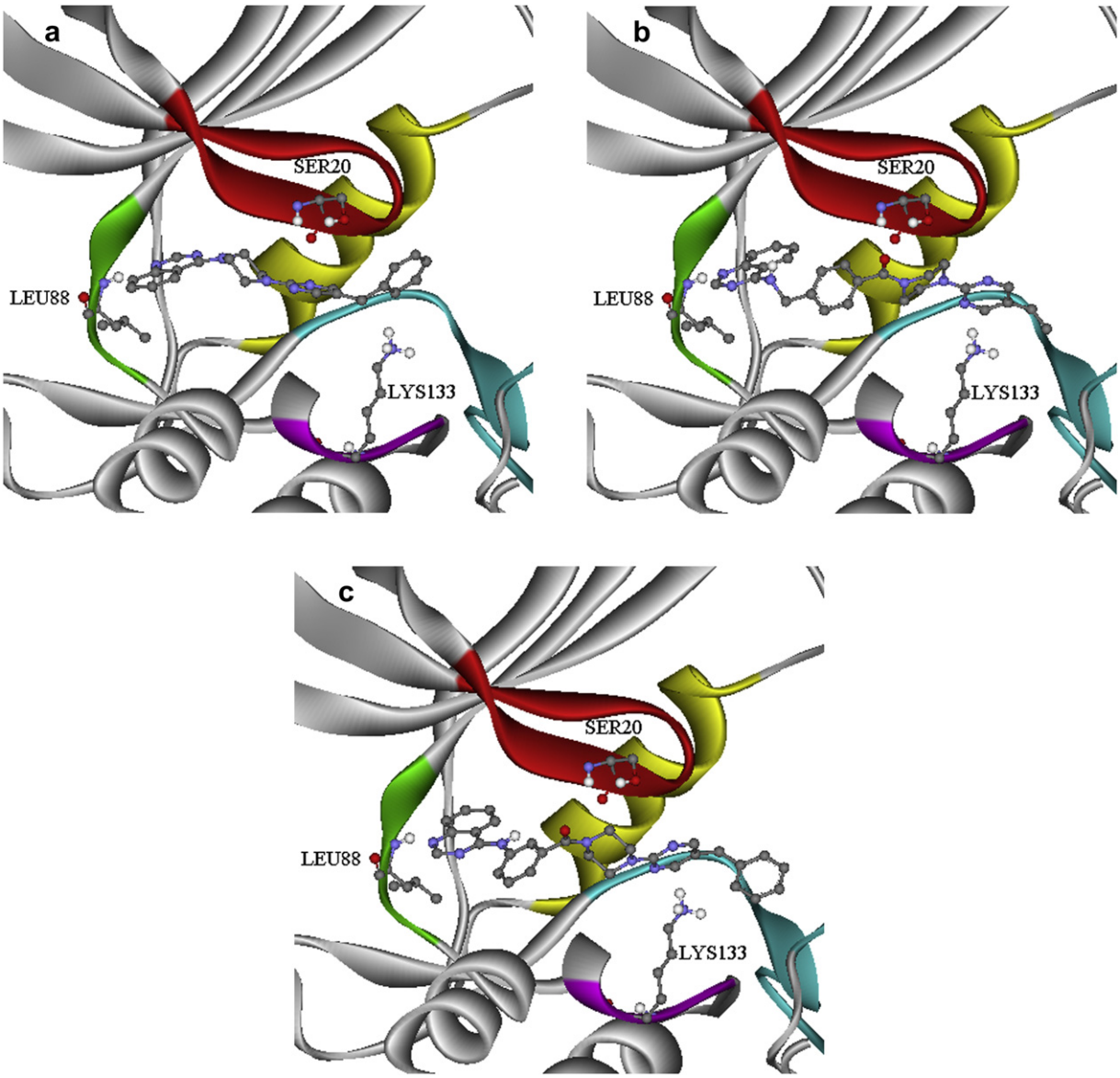

Fig. 4. The results from the docking simulation of **4** (**a**), **15** (**b**), and **16** (**c**), with CSNK1D (PDB: 1CKI). The protein is represented as a solid ribbon. The SER20, LEU88, LYS133, **4**, **15**, and **16** are shown as ball and stick representation. The hinge region is colored green, the β6 strand is colored magenta, the β9 strand is colored in cyan, the P-loop is colored in red, and the αA-helix is colored in yellow. The pictures were prepared using DS ViewerPro 6.0 software. The predicted binding mode of both **15** and **16** was the same among the top ranked energy cluster whereas that of **4** belongs to the second ranked energy cluster. (For interpretation of the references to colour in this figure legend, the reader is referred to the web version of this article.).

behavior of the three compounds toward binding and inhibiting the function of certain kinase subfamilies. Compound **4** showed an additional interesting feature of binding to or inhibiting the function of certain KIT and PDGFR mutants compared to their wild-type isoforms. The last observation strengthen the hypothesis that **4** may act as a type-I kinase inhibitor based on a comparison with 38 kinase inhibitors and molecular docking experiments. Piperazinylpyrimidine based derivatives have been shown through this report to have the potential of being lead selective kinase inhibitors as well as optimized selective antiproliferative agents.

3. Experimental section

3.1. Chemistry

3.1.1. General methods

All temperatures are expressed in °C (degrees centigrade). All reagents, solvents, and starting materials were obtained from commercial suppliers and used without further purification. Reactions requiring anhydrous conditions were performed in dry solvents under Argon atmosphere. Reactions were monitored by thin layer chromatography (TLC) on precoated silica gel F_{254} plates (EMD) using a UV detector for visualization. Flash column chromatography was performed with EMD 230–400 mesh silica gel 60 Å. Yields are of purified products. Melting points were determined using Thomas Hoover melting point apparatus and are uncorrected. ^{1}H NMR and ^{13}C-NMR spectra were recorded on a Jeol JNM–ECA600 spectrometer. The obtained FID of each experiment was processed using Delta NMR 1D processor software. The chemical shifts are expressed in parts per million (ppm, δ) down field from TMS. Spin multiplicities are designated as s (singlet), d (doublet), dd (doublet of doublets), ddd (doublet of doublet of doublets), t (triplet), q (quartet), m (multiplet), and br (broad). Mass spectra (MS) were determined by MALDI instrument. 1 μL test compound solution in acetonitrile is mixed with an equal amount of the matrix solution (saturated

2,5-dihydroxybenzoic acid in 50% ethanol) on the MALDI plate. MALDI spectra were recorded in positive reflectron mode on an AXIMA curved-field reflectron (CFR) MALDI-TOF mass spectrometer (Kratos/Shimadzu, Columbia, MD, USA). Analytical HPLC was performed using a C18 Phenomenex quantitative 5 μm 4.6 mm × 150 mm column with a 30 min gradient of solvent from 10% to 90% CH_3CN in H_2O. Retention time (R_t) was recorded in minutes and purity was indicated as percentage of the target compound calculated from % area under the peak (AEP). All final purified compounds showed purity levels greater than 95%.

*3.1.2. 5-Ethyl-2-(piperazin-1-yl)pyrimidine (**1**)*

a) A mixture of tert-butyl piperazine-1-carboxylate (6.5 gm, 35.2 mmol), 2-chloro-4-ethylpyrimidine (5 gm, 35.2 mmol), triethylamine (3.55 gm, 35.2 mmol), and absolute ethanol (60 ml) were refluxed for 12 h and then cooled. Ice water was added and the resulting precipitate was filtered, washed with cold water, and finally dried to afford the desired crude intermediate, tert-butyl 4-(5-ethylpyrimidin-2-yl)piperazine-1-carboxylate, as white flakes (9.24 gm, 90% yield); mp: 67–68 °C ^{1}H NMR (DMSO-*d6*): δ 1.19 (t, J = 7.56 Hz, 3H), 1.46 (s, 9H), 2.47 (q, J = 7.56 Hz, 2H), 3.49 (t, J = 4.8 Hz, 4H), 3.76 (t, J = 4.8 Hz, 4H), 8.19 (s, 2H). ^{13}C NMR (DMSO-*d6*): δ 15.59, 22.66, 28.4, 43.76, 43.77, 79.8, 124.95, 154.84, 157.08, 160.05. MS: calcd 292.19 for $C_{15}H_{24}N_4O_2$ $[M]^+$; found, 293.19 $[M + 1]^+$. b) HCl/MeOH mixture was prepared by adding10 ml acetyl chloride dropwise to 100 ml methanol at 0 °C. The resulting mixture was warmed to room temperature. The intermediate from step a (9 gm, 30.8 mmol) was then added to the HCl/MeOH and stirred for 12 h at room temperature. Methanol was removed using a rotary evaporator. The residue was dissolved in water; the solution was neutralized using solid $NaHCO_3$. The mixture was extracted with $CHCl_3$ (3 × 200 mL). The combined organic layers was washed successively with saturated $NaHCO_3$, and saturated brine and then dried with anhydrous Na_2SO_4. Concentration of the organic layer afforded the desired crude product **1** as a white solid (4.8 gm, 81% yield); mp: 115–116 °C ^{1}H NMR (DMSO-*d6*): δ 1.20 (t, J = 7.56 Hz, 3H), 2.48 (q, J = 7.56 Hz, 2H), 3.09 (t, J = 5.16 Hz, 4H), 3.94 (t, J = 5.16 Hz, 4H), 8.19 (s, 2H). ^{13}C NMR (DMSO-*d6*): δ 15.53, 22.67, 42.76, 44.30, 125.52, 157.15, 160.09.

*3.1.3. 5-Benzyl-2-(piperazin-1-yl)pyrimidine (**2**)*

a) A mixture of K_2CO_3 (6 gm, 43.5 mmol, 3 equiv) and $Pd(PPh_3)_4$ (1 gm, 0.86 mmol) were stirred at room temperature in 20 mL THF/water (1:1) for 30 min. Tert-butyl 4-(5-bromopyrimidin-2-yl) piperazine-1-carboxylate (5 gm, 14.5 mmol, 1 equiv) was then added with *B*-benzyl-9-BBN (2 equiv, 49 ml of a 0.5 M solution in THF). The resulting mixture was heated with stirring under argon atmosphere in an oil bath adjusted at 100–110 °C until the reaction had reached completion, as monitored by TLC. The reaction mixture was extracted with $CHCl_3$ (3 × 200 mL). The combined organic layers were then dried with anhydrous Na_2SO_4. Chloroform was evaporated under reduced pressure and the residue was purified using flash column chromatography (initially with 4:1 hexane/ethylacetate and finally with 1:1 hexane/ethylacetate). Tert-butyl 4-(5-benzylpyrimidin-2-yl)piperazine-1-carboxylate was obtained as a yellow solid (3.8 gm, 74% yield); mp: 121–123 °C ^{1}H NMR (DMSO-*d6*): δ 1.47 (s, 9H), 3.47 (t, J = 4.68 Hz, 4H), 3.75 (t, J = 4.68 Hz, 4H), 3.78 (s, 2H), 7.14–7.29 (m, 5H), 8.16 (s, 2H). ^{13}C NMR (DMSO-*d6*): δ 28.4, 35.61, 43.70, 79.92, 122.29, 126.41, 128.51, 128.66, 140.02, 154.84, 157.87, 160.69. MS: calcd 354.21 for $C_{20}H_{26}N_4O_2$ $[M]^+$; found, 355.21 $[M + 1]^+$. b) 3.7 gm of the obtained product from step a was then deprotected using HCl/MeOH as described above in the preparation of 1. As a result, compound **2** was obtained as a pale yellow solid (2.2 gm, 80% yield); mp: 108–110 °C ^{1}H NMR (DMSO-*d6*): δ 1.89 (s, 1H), 2.93 (t, J = 4.8 Hz, 4H), 3.76 (t, J = 4.8 Hz, 4H), 3.79 (s, 2H), 7.17–7.29 (m, 5H), 8.18 (s, 2H). ^{13}C NMR (DMSO-*d6*): δ 35.59, 44.96, 45.92, 121.79, 126.34, 128.48, 128.6, 140.1, 157.8, 160.5. MS: calcd 254.15 for $C_{15}H_{18}N_4$ $[M]^+$; found, 255.15 $[M + 1]^+$.

*3.1.4. 4-(4-(5-Ethylpyrimidin-2-yl)piperazin-1-yl)quinazoline (**3**)*

A mixture of **1** (72 mg, 0.377 mmol), 4-chloroquinzoline (61 mg, 0.377 mmol), and triethylamine (38 mg, 0.377 mmol) in isopropanol (5 ml) was refluxed at 80 °C for 1.5 h. The solid separated out of the reaction was filtered, washed with hot solvent and dried to afford compound **3** which was obtained as a yellow solid (61 mg, 50% yield); mp: >250 °C. The purity of **3** was confirmed using HPLC (97.27%, R_t = 9.987). ^{1}H NMR (DMSO-*d6*): δ 1.13 (t, J = 7.56 Hz, 3H), 2.45 (q, J = 7.56 Hz, 2H), 3.95 (t, J = 5.28 Hz, 4H), 4.16 (t, J = 5.28 Hz, 4H), 7.68 (ddd, J = 1.38 Hz, J = 6.84 Hz, J = 8.4 Hz, 1H), 7.96 (m, 2H), 8.22 (d, J = 8.4 Hz, 1H), 8.31 (s, 2H), 8.82 (s, 1H). ^{13}C NMR (DMSO-*d6*): δ 15.63, 21.91, 42.85, 48.78, 113.28, 121.66, 125.04, 126.69, 126.88, 134.78, 143.5, 149.89, 157.19, 159.95, 162.51. MS: calcd 320.17 for $C_{18}H_{20}N_6$ $[M]^+$; found, 320.39 $[M]^+$.

*3.1.5. 4-(4-(5-Benzylpyrimidin-2-yl)piperazin-1-yl)quinazoline (**4**)*

Compound **4** was prepared from **2** (90 mg, 0. 354 mmol) and 4-chloroquinzoline (58 mg, 0. 354 mmol) following the same procedure for the preparation of **3**. The product was a yellow solid (86 mg, 63%); mp: >250 °C. The purity of **4** was confirmed using HPLC (97.59%, R_t = 15.025).^{1}H NMR (DMSO-*d6*): δ 3.8 (s, 2H), 3.96 (t, J = 5.16 Hz, 4H), 4.26 (t, J = 5.16 Hz, 4H), 7.17–7.3 (m, 5H), 7.71 (ddd, J = 2.22 Hz, J = 6.36 Hz, J = 8.4 Hz, 1H), 8.01 (m, 2H), 8.25 (d, J = 8.4 Hz, 1H), 8.34 (s, 2H), 8.86 (s, 1H). ^{13}C NMR (DMSO-*d6*): δ 34.51, 42.6, 48.69, 112.49, 119.73, 123.03, 126.11, 126.98, 127.32, 128.32, 128.54, 135.36, 140.86, 140.96, 148.74, 157.84, 159.77, 162.12. MS: calcd 382.19 for $C_{23}H_{22}N_6$ $[M]^+$; found, 383.35 $[M + 1]^+$.

*3.1.6. 4-(4-(5-Ethylpyrimidin-2-yl)piperazin-1-yl)-2-phenylquinazoline (**5**)*

Compound **5** was prepared from **1** (72 mg, 0.377 mmol) and 2-phenyl-4-chloroquinzoline (90 mg, 0.377 mmol) following the same procedure for the preparation of **3**. The product was a white solid (100 mg, 67%); mp: 137–138 °C. The purity of **5** was confirmed using HPLC (96.43%, R_t = 15.09). ^{1}H NMR (DMSO-*d6*): δ 1.14 (t, J = 7.56 Hz, 3H), 2.44 (q, J = 7.56 Hz, 2H), 3.93–3.98 (m, 8H), 7.50–7.54 (m, 4H), 7.83 (ddd, J = 1.38 Hz, J = 6.84 Hz, J = 8.28 Hz, 1H), 7.9 (dd, J = 0.96 Hz, J = 8.28 Hz, 1H), 8.1 (dd, J = 0.96 Hz, J = 8.28 Hz, 1H), 8.3 (s, 2H), 8.51 (m, 2H). ^{13}C NMR (DMSO-*d6*): δ 15.6, 21.93, 43.33, 48.85, 114.75, 119.3, 123.55, 125.36, 125.4, 127.96, 128.37, 130.31, 132.9, 138.03, 152.11, 157.13, 158.08, 160.36, 164.12. MS: calcd 396.21 for $C_{24}H_{24}N_6$ $[M]^+$; found, 397.4 $[M + 1]^+$.

*3.1.7. 4-(4-(5-Benzylpyrimidin-2-yl)piperazin-1-yl)-2-phenylquinazoline (**6**)*

Compound **6** was prepared from **2** (90 mg, 0.354 mmol) and 2-phenyl-4-chloroquinzoline (84 mg, 0.354 mmol) following the same procedure for the preparation of **3**. The product was a white solid (160 mg, 98%); mp: 135–137 °C.The purity of **6** was confirmed using HPLC (98.57%, R_t = 19.707). ^{1}H NMR (DMSO-*d6*): δ 3.79 (s, 2H), 3.91–3.96 (m, 8H), 7.17–7.30 (m, 5H), 7.49–7.54 (m, 4H), 7.82 (ddd, J = 0.78 Hz, J = 6.6 Hz, J = 7.92 Hz, 1H), 7.9 (d, J = 8.28 Hz, 1H), 8.08 (d, J = 8.28 Hz, 1H), 8.32 (s, 2H), 8.51 (m, 2H). ^{13}C NMR (*DMSO-d6*): δ 34.56, 43.24, 48.81, 114.74, 122.82, 125.35, 125.4, 126.11, 127.95, 128.35, 128.56, 130.32, 132.89, 138.02, 140.9, 152.11, 157.81, 158.06, 160.26, 164.09. MS: calcd 458.22 for $C_{29}H_{26}N_6$ $[M]^+$; found, 458.28 $[M]^+$.

*3.1.8. General preparation of quinazoline-4-ylaminobenzoic acid and quinazoline-4-ylaminomethylbenzoic acid intermediates (**7**–**12**)*

Either 4-chloroquinzoline or 2-phenyl-4-chloroquinzoline was reacted with an equivalent amount of the corresponding aminobenzoic acid or aminomethylbenzoic acid derivative in the presence of an equivalent amount of triethylamine using anhydrous isopropanol as a solvent. The reaction was performed under 80 °C until the starting materials were consumed. The solid furnished out of the reaction, after solvent evaporation, was washed with hot water to remove triethylamine HCl and used in the next step without any further purification.

*3.1.9. 3-(quinazolin-4-ylamino)benzoic acid (**7**)*

This intermediate is commercially available and is also reported [69–71]. ^{1}H NMR (DMSO-*d6*): δ 7.61 (t, *J* = 7.92 Hz, 1H), 7.84–7.88 (m, 2H), 8.00–8.1 (m, 3H), 8.38 (t, *J* = 1.74 Hz, 1H), 8.91 (s, 1H), 8.96 (d, *J* = 8.28, 1H). ^{13}C NMR (DMSO-*d6*): δ 113.69, 121.06, 124.49, 124.86, 126.55, 128.02, 128.34, 128.74, 131.25, 135.47, 137.31, 140.61, 151.42, 159.4, 166.62. MS: calcd 265.09 for $C_{15}H_{11}N_3O_2$ $[M]^+$; found, 265.6 $[M]^+$.

*3.1.10. 4-(quinazolin-4-ylamino)benzoic acid (**8**)*

This intermediate is commercially available and is also reported [70–72]. ^{1}H NMR (DMSO-*d6*): δ 7.75–7.77 (m, 1H), 7.91–8.05 (m, 6H), 8.83–8.84 (m, 2H). ^{13}C NMR (DMSO-*d6*): δ 115.08, 123.12, 124.43, 124.66, 127.32, 128.13, 130.44, 135.32, 142.76, 144.92, 153.12, 159.25, 167.34. MS: calcd 265.09 for $C_{15}H_{11}N_3O_2$ $[M]^+$; found, 265.7 $[M]^+$.

*3.1.11. 4-((quinazolin-4-ylamino)methyl)benzoic acid (**9**)*

This intermediate is commercially available and is also reported [73]. ^{1}H NMR (DMSO-*d6*): δ 4.86 (d, *J* = 5.88 Hz, 2H), 7.46 (d, *J* = 8.64 Hz, 2H), 7.54 (ddd, *J* = 1.2 Hz, *J* = 7.08 Hz, *J* = 8.28 Hz, 1H), 7.7 (dd, *J* = 0.84 Hz, *J* = 7.56 Hz, 1H), 7.78 (ddd, *J* = 1.2 Hz, *J* = 6.9 Hz, *J* = 8.22 Hz, 1H), 7.89 (d, *J* = Hz, 2H), 8.31 (dd, *J* = 0.84 Hz, *J* = 7.56 Hz, 1H), 8.44 (s, 1H), 8.93 (t, *J* = 5.88 Hz, 1H). ^{13}C NMR (DMSO-*d6*): δ 46.91, 115.41, 123.19, 126.35, 127.64, 128.07, 129.83, 129.95, 133.23, 145.23, 149.66, 155.54, 159.91, 167.73. MS: calcd 279.1 for $C_{16}H_{13}N_3O_2$ $[M]^+$; found, 279.5 $[M]^+$.

*3.1.12. 3-(2-Phenylquinazolin-4-ylamino)benzoic acid (**10**)*

This intermediate is commercially available and is also reported [74]. ^{1}H NMR (DMSO-*d6*): δ 7.54–7.80 (m, 6H), 7.94–7.96 (m, 2H), 8.19–8.21 (m, 1H), 8.52–8.54 (m, 2H), 8.67–8.69 (m, 1H), 8.93 (s, 1H). MS: calcd 341.12 for $C_{21}H_{15}N_3O_2$ $[M]^+$; found, 341.6 $[M]^+$.

*3.1.13. 4-(2-Phenylquinazolin-4-ylamino)benzoic acid (**11**)*

This intermediate is commercially available and is also reported [74,75]. ^{1}H NMR (DMSO-*d6*): δ 7.55–7.58 (m, 3H), 7.7–7.73 (m, 1H), 7.96–8.08 (m, 6H), 8.39–8.4 (m, 2H), 8.73–8.74 (s, 1H). ^{13}C NMR (*DMSO-d6*): δ 114.10, 122.91, 124.38, 127.07, 127.71, 129.11, 129.32, 130.56, 132.29, 135.26, 142.99, 158.77, 158.99, 167.41. MS: calcd 341.12 for $C_{21}H_{15}N_3O_2$ $[M]^+$; found, 341.7 $[M]^+$.

*3.1.14. 4–((2-Phenylquinazolin-4-ylamino)methyl)benzoic acid (**12**)*

The product was a white solid (37%); mp: 272 °C ^{1}H NMR (DMSO-*d6*): δ 4.97 (d, *J* = 5.82 Hz, 2H), 7.44–7.56 (m, 4H), 7.79 (m, 2H), 7.89 (m, 3H), 8.31 (m, 1H), 8.40 (m, 2H), 8.85 (t, *J* = 5.82 Hz, 1H). ^{13}C NMR (DMSO-*d6*): δ 43.66, 113.66, 122.49, 125.18, 127.01, 127.15, 127.68, 127.91, 129.01, 129.13, 129.73, 130, 132.53, 138.46, 144.41, 149.91, 159.08, 159.51, 167.05. MS: calcd 355.13 for $C_{22}H_{17}N_3O_2$ $[M]^+$; found, 355.6 $[M]^+$.

*3.1.15. (4-(5-Ethylpyrimidin-2-yl)piperazin-1-yl)(3-(quinazolin-4-ylamino)phenyl)methanone (**13**)*

Intermediate **1** (72 mg, 0.377 mmol) was reacted with intermediate **7** (99 mg, 0.377 mmol) in the presence of equivalent amounts of both EDC.HCl (72 mg, 0.377 mmol) and TEA (38 mg, 0.377 mmol) using 5 ml of CH_2Cl_2 as a solvent. The reaction mixture was stirred under room temperature overnight. The solvent was evaporated under pressure and the title compound was purified using flash column chromatography (2.5% MeOH in CH_2Cl_2). The product was a white solid (107 mg, 64%); mp: 146–147 °C. The purity of **13** was confirmed using HPLC (97.1%, R_t = 11.075). ^{1}H NMR (DMSO-*d6*): δ 1.12 (t, *J* = 7.44 Hz, 3H), 2.43 (q, *J* = 7.44 Hz, 2H), 3.35–3.79 (br, m, 8H), 7.2 (dd, *J* = 1.2 Hz, *J* = 7.74 Hz, 1H), 7.48 (t, *J* = 7.92 Hz, 1H), 7.65 (ddd, *J* = 1.38 Hz, *J* = 7.38 Hz, *J* = 8.28 Hz, 1H), 7.8 (dd, *J* = 1.2 Hz, *J* = 7.38 Hz, 1H), 7.87 (ddd, *J* = 1.38 Hz, *J* = 7.08 Hz, *J* = 8.28 Hz, 1H), 7.98 (ddd, *J* = 0.72 Hz, *J* = 1.8 Hz, *J* = 8.28 Hz, 1H), 8.02 (t, *J* = 1.68 Hz, 1H), 8.27 (s, 2H), 8.57 (dd, *J* = 0.72 Hz, *J* = 7.74 Hz, 1H), 8.63 (s, 1H), 9.93 (s, 1H). ^{13}C NMR (DMSO-*d6*): δ 15.58, 21.9, 41.49, 43.34, 43.87, 46.95, 115.16, 120.82, 122.17, 122.97, 123.18, 125.01, 126.38, 127.85, 128.67, 133.13, 135.88, 139.23, 149.7, 154.36, 157.13, 157.67, 160.24, 169.02. MS: calcd 439.21 for $C_{25}H_{25}N_7O$ $[M]^+$; found, 439.12 $[M]^+$.

*3.1.16. (4-(5-Ethylpyrimidin-2-yl)piperazin-1-yl)(4-(quinazolin-4-ylamino)phenyl)methanone (**14**)*

Compound **14** was prepared from intermediate **1** (72 mg, 0.377 mmol) and intermediate **8** (99 mg, 0.377 mmol) following the same procedure utilized in the preparation of **13**. The product obtained was a white solid (100 mg, 60%); mp: 248–249 °C. The purity of **14** was confirmed using HPLC (95%, R_t = 10.753). ^{1}H NMR (DMSO-*d6*): δ 1.12 (t, *J* = 7.56 Hz, 3H), 2.43 (q, *J* = 7.56 Hz, 2H), 3.33–3.84 (br, m, 8H), 7.5 (d, *J* = 8.64 Hz, 2H), 7.66 (ddd, *J* = 1.38, Hz, *J* = 7.2 Hz, *J* = 8.28 Hz, 1H), 7.82 (d, *J* = 8.28 Hz, 1H), 7.88 (ddd, *J* = 1.38 Hz, *J* = 7.2 Hz, *J* = 8.28 Hz, 1H), 8.02 (d, *J* = 8.64 Hz, 2H), 8.27 (s, 2H), 8.59 (d, *J* = 8.46 Hz, 1H), 8.66 (s, 1H), 9.93 (s, 1H). ^{13}C NMR (DMSO-*d6*): δ 15.53, 21.87, 41.55, 43.6, 46.95, 115.19, 121.34, 122.99, 124.92, 126.37, 127.62, 127.78, 127.84, 130.37, 133.12, 140.57, 149.72, 154.2, 157.1, 157.55, 160.2, 169.08. MS: calcd 439.21 for $C_{25}H_{25}N_7O$ $[M]^+$; found, 439.16 $[M]^+$.

*3.1.17. (4-(5-Ethylpyrimidin-2-yl)piperazin-1-yl)(4-((quinazolin-4-ylamino)methyl)phenyl)methanone (**15**)*

Compound **15** was prepared from intermediate **1** (77 mg, 0.405 mmol) and intermediate **9** (113 mg, 0.405 mmol) following the general procedure used in the preparation of **13**. The product obtained was a white solid (40 mg, 21%); mp: 170–171 °C. The purity of **15** was confirmed using HPLC (95.48%, R_t = 11.288). ^{1}H NMR (DMSO-*d6*): δ 1.11 (t, *J* = 7.56 Hz, 3H), 2.42 (q, *J* = 7.56 Hz, 2H), 3.34–3.76 (br, m, 8H), 4.84 (d, *J* = 5.82 Hz, 2H), 7.4 (d, *J* = 8.4 Hz, 2H), 7.44 (d, *J* = 8.4 Hz, 2H), 7.54 (ddd, *J* = 1.2 Hz, *J* = 6.72 Hz, *J* = 8.28 Hz, 1H), 7.7 (dd, *J* = 0.84 Hz, *J* = 7.56 Hz, 1H), 7.78 (ddd, *J* = 1.2 Hz, *J* = 6.72 Hz, *J* = 8.28 Hz, 1H), 8.26 (s, 2H), 8.31 (dd, *J* = 0.84 Hz, *J* = 7.56 Hz, 1H), 8.46 (s, 1H), 8.9 (t, *J* = 5.82 Hz, 1H). ^{13}C NMR (DMSO-*d6*): δ 15.58, 21.89, 43.25, 43.75, 46.92, 114.88, 122.63, 124.97, 125.77, 127.09, 127.23, 127.57, 132.67, 134.27, 141.11, 149.17, 155.05, 157.12, 159.37, 160.18, 169.13. MS: calcd 453.23 for $C_{26}H_{27}N_7O$ $[M]^+$; found, 453 $[M]^+$.

*3.1.18. (4-(5-Benzylpyrimidin-2-yl)piperazin-1-yl)(3-(quinazolin-4-ylamino)phenyl)methanone (**16**)*

Compound **16** was prepared from intermediate **2** (90 mg, 0.354 mmol) and intermediate **7** (93 mg, 0.354 mmol) following the same procedure utilized in the preparation of **13**. The product obtained was a white solid (125 mg, 70%); mp: 120–122 °C. The purity of **16** was confirmed using HPLC (97.17%, R_t = 15.488). ^{1}H

NMR (DMSO-*d6*): δ 3.34–3.78 (br, m, 10H), 7.17–7.29 (m, 6H), 7.48 (t, *J* = 7.92 Hz, 1H), 7.65 (ddd, *J* = 0.96 Hz, *J* = 6.96 Hz, *J* = 8.88 Hz, 1H), 7.8 (d, *J* = 7.56 Hz, 1H), 7.87 (m. 1H), 7.98 (m, 1H), 8.02 (s, 1H), 8.31 (s, 2H), 8.56 (d, *J* = 7.92 Hz, 1H), 8.62 (s, 1H), 9.92 (s, 1H). ^{13}C NMR (DMSO-*d6*): δ 34.53, 41.5, 43.25, 43.78, 46.9, 115.15, 120.82, 122.17, 122.96, 123.18, 126.12, 126.38, 127.86, 128.34, 128.56, 128.67, 133.13, 139.23, 140.87, 149.7, 154.36, 157.67, 157.81, 160.17, 169.02. MS: calcd 501.23 for $C_{30}H_{27}N_7O$ [M]$^+$; found, 501.95 [M] $^+$.

3.1.19. (4-(5-Benzylpyrimidin-2-yl)piperazin-1-yl)(4-(quinazolin-4-ylamino)phenyl)methanone (**17**)

Compound **17** was prepared from intermediate **2** (90 mg, 0.354 mmol) and intermediate **8** (93 mg, 0.354 mmol) following the procedure used in the preparation of compound **13**. The product obtained was a white solid (135 mg, 76%); mp: 245–247 °C. The purity of **17** was confirmed using HPLC (96.73%, R_t = 14.952). ^{1}H NMR (DMSO-*d6*): δ 3.05–3.8 (br, m, 10H), 7.18–7.31 (m, 5H), 7.5 (d, *J* = 8.64 Hz, 2H), 7.67 (ddd, *J* = 1.38, Hz, *J* = 7.2 Hz, *J* = 8.1 Hz, 1H), 7.82 (d, *J* = 8.28 Hz, 1H), 7.89 (ddd, *J* = 1.2 Hz, *J* = 6.96 Hz, *J* = 8.28 Hz, 1H), 8.04 (d, *J* = 8.64 Hz, 2H), 8.32 (s, 2H), 8.65 (d, *J* = 8.1 Hz, 1H), 8.67 (s, 1H), 10.01 (s, 1H). ^{13}C NMR (DMSO-*d6*): δ 34.50, 43.52, 45.38, 115.20, 121.73, 122.87, 123.11, 126.08, 126.35, 127.75, 127.8, 128.3, 128.51, 130.34, 133.12, 140.59, 140.83, 149.69, 154.27, 157.57, 157.78, 160.13, 169.09. MS: calcd 501.23 for $C_{30}H_{27}N_7O$ [M]$^+$; found, 501.74 [M] $^+$.

3.1.20. (4-(5-Benzylpyrimidin-2-yl)piperazin-1-yl)(4-((quinazolin-4-ylamino)methyl)phenyl)methanone (**18**)

Compound **18** was prepared from intermediate **2** (102 mg, 0.405 mmol) and intermediate **9** (113 mg, 0.405 mmol) following the general procedure used in the preparation of **13**. The product obtained was a white solid (40 mg, 19%); mp: 99–101 °C. The purity of **18** was confirmed using HPLC (96.14%, R_t = 15.95). ^{1}H NMR (DMSO-*d6*): δ 3.37–3.83 (br, m, 10H), 4.89 (d, *J* = 5.82 Hz, 2H), 7.22–7.34 (m, 5H), 7.43 (d, *J* = 8.28 Hz, 2H), 7.49 (d, *J* = 8.28 Hz, 2H), 7.6 (ddd, *J* = 1.2 Hz, *J* = 6.72 Hz, *J* = 8.28 Hz, 1H), 7.76 (dd, *J* = 0.84 Hz, *J* = 7.56 Hz, 1H), 7.84 (ddd, *J* = 1.2 Hz, *J* = 6.72 Hz, *J* = 8.28 Hz, 1H), 8.34 (s, 2H), 8.36 (d, *J* = 7.92 Hz, 1H), 8.51 (s, 1H), 8.94 (t, *J* = 5.82 Hz, 1H). ^{13}C NMR (DMSO-*d6*): δ 34.49, 43.23, 114.86, 122.61, 122.89, 125.74, 126.09, 127.07, 127.2, 127.54, 128.31, 128.53, 132.62, 134.23, 140.83, 141.09, 149.17, 155.02, 157.77, 159.36, 160.1, 169.1. MS: calcd 515.24 for $C_{31}H_{29}N_7O$ [M]$^+$; found, 515 [M] $^+$.

3.1.21. (4-(5-Ethylpyrimidin-2-yl)piperazin-1-yl)(2-(3-phenylquinazolin-4-ylamino)phenyl)methanone (**19**)

Compound **19** was prepared from intermediate **1** (120 mg, 0.625 mmol) and intermediate **10** (213 mg, 0.625 mmol) following the same procedure utilized in the preparation of **13**. The product obtained was a white solid (210 mg, 40%); mp: 204–205 °C. The purity of **19** was confirmed using HPLC (97.67%, R_t = 15.123). ^{1}H NMR (DMSO-*d6*): δ 1.09 (t, 3H), 2.4 (q, 2H), 3.16–3.71 (m, 8H), 7.18 (d, *J* = 7.56 Hz, IH), 7.41–7.59 (m, 5H), 7.83 (m, 2H), 8.02 (m, 1H), 8.13 (m, 1H), 8.21 (s, 2H), 8.4 (m, 2H), 8.54 (d, *J* = 8.22 Hz, 1H), 9.87 (s, 1H). ^{13}C NMR (DMSO-*d6*): δ 15.36, 21.85, 42.66, 44.25, 114.01, 120.67, 121.79, 122.86, 125.02, 125.97, 127.9, 128.16, 128.27, 128.6, 130.12, 130.2, 133.23, 136.23, 138.3, 139.59, 150.56, 157.03, 157.92, 159.02, 160.3, 169.2. MS: calcd 515.24 for $C_{31}H_{29}N_7O$ [M]$^+$; found, 515.84 [M] $^+$.

3.1.22. (4-(5-Ethylpyrimidin-2-yl)piperazin-1-yl)(2-(4-phenylquinazolin-4-ylamino)phenyl)methanone (**20**)

Compound **20** was prepared from intermediate **1** (120 mg, 0.625 mmol) and intermediate **11** (213 mg, 0.625 mmol) following the same procedure utilized in the preparation of **13**. The product obtained was a white solid (180 mg, 34%); mp: >250 °C. The purity of **20** was confirmed using HPLC (96.02%, R_t = 14.823). ^{1}H NMR (DMSO-*d6*): δ 1.12 (t, 3H), 2.43 (q, 2H), 3.32–3.78 (m, 8H), 7.51–7.65 (m, 6H), 7.89 (m, 2H), 8.12 (m, 2H), 8.27 (s, 2H), 8.47 (m, 2H), 8.6 (d, *J* = 8.28 Hz, 1H), 10.0 (s, 1H). ^{13}C NMR (DMSO-*d6*): δ 15.54, 21.88, 43.59, 114.04, 121.22, 123.07, 124.92, 126.07, 127.91, 128.17, 128.47, 130.28, 130.33, 133.36, 138.16, 140.74, 150.53, 157.1, 157.77, 158.94, 160.22, 169.11. MS: calcd 515.24 for $C_{31}H_{29}N_7O$ [M]$^+$; found, 515.89 [M] $^+$.

3.1.23. (4-(5-Ethylpyrimidin-2-yl)piperazin-1-yl)(4–((2-phenylquinazolin-4 ylamino)methyl)phenyl)methanone (**21**)

Compound **21** was prepared from intermediate **1** (120 mg, 0.625 mmol) and intermediate **12** (221 mg, 0.625 mmol) following the same procedure utilized in the preparation of **13**. The product obtained was a white solid (105 mg, 20%); mp: 207–208 °C. The purity of **21** was confirmed using HPLC (97.08%, R_t = 15.735). ^{1}H NMR (DMSO-*d6*): δ 1.1 (t, 3H), 2.41 (q, 2H), 3.34–3.76 (m, 8H), 4.97 (d, *J* = 5.82 Hz, 2H), 7.4–7.55 (m, 8H), 7.79 (m, 2H), 8.25 (s, 2H), 8.33 (m, 1H), 8.43 (m, 2H), 8.98 (t, *J* = 5.82 Hz, 1H). ^{13}C NMR (DMSO-*d6*): δ 15.56, 21.88, 41.4, 43.26, 43.56, 46.85, 113.79, 122.68, 124.94, 125.45, 127.24, 127.31, 127.84, 128.2, 130.3, 132.83, 134.26, 138.52, 141.51, 149.98, 157.1, 159.15, 159.59, 160.16, 169.11. MS: calcd 529.26 for $C_{32}H_{31}N_7O$ [M]$^+$; found, 529.88 [M] $^+$.

3.1.24. (4-(5-Benzylpyrimidin-2-yl)piperazin-1-yl)(3-(2-phenylquinazolin-4-ylamino)phenyl)methanone (**22**)

Compound **22** was prepared from intermediate **2** (120 mg, 0.472 mmol) and intermediate **10** (160 mg, 0.472 mmol) following the same procedure utilized in the preparation of **13**. The product obtained was a white solid (135 mg, 23%); mp: 214–215 °C. The purity of **22** was confirmed using HPLC (95.38%, R_t = 18.948). ^{1}H NMR (DMSO-*d6*): δ 3.37–3.83 (br, m, 10H), 7.2–7.32 (m, 6H), 7.44–7.67 (m, 5H), 7.91 (m, 2H), 8.1 (ddd, *J* = 0.9 Hz, *J* = 2.1 Hz, *J* = 8.28 Hz, 1H), 8.2 (m, 1H), 8.32 (s, 2H), 8.47 (m, 2H), 8.62 (d, *J* = 8.28 Hz, 1H), 10.0 (s, 1H). ^{13}C NMR (DMSO-*d6*): δ 34.53, 41.46, 43.84, 46.95, 113.99, 120.65, 121.84, 122.89, 122.98, 123.02, 126.07, 126.11, 127.88, 128.17, 128.33, 128.54, 128.66, 128.78, 130.3, 131.43, 132.01, 133.34, 136.11, 138.18, 139.54, 140.85, 150.49, 157.77, 157.85, 158.92, 160.15, 169.14. MS: calcd 577.26 for $C_{36}H_{31}N_7O$ [M]$^+$; found, 577.55 [M] $^+$.

3.1.25. (4-(5-Benzylpyrimidin-2-yl)piperazin-1-yl)(4-(2-phenylquinazolin-4-ylamino)phenyl)methanone (**23**)

Compound **23** was prepared from intermediate **2** (120 mg, 0.472 mmol) and intermediate **11** (160 mg, 0.472 mmol) following the same procedure utilized in the preparation of **13**. The product obtained was a white solid (70 mg, 12%); mp: >250 °C. The purity of **23** was confirmed using HPLC (95%, R_t = 18.98). ^{1}H NMR (DMSO-*d6*): δ 3.38–3.82 (br, m, 10H), 7.21–7.33 (m, 6H), 7.53–7.69 (m, 5H), 7.93 (m, 2H), 8.15 (m. 2H), 8.34 (s, 2H), 8.51 (m, 2H), 8.64 (d, *J* = 8.28 Hz, 1H), 10.06 (s, 1H). ^{13}C NMR (DMSO-*d6*): δ 34.56, 43.53, 114.08, 121.28, 122.95, 123.11, 126.16, 127.98, 128.21, 128.38, 128.54, 128.6, 128.75, 130.29, 130.42, 131.47, 133.44, 138.19, 140.8, 140.89, 150.57, 157.83, 159, 160.18, 169.19. MS: calcd 577.26 for $C_{36}H_{31}N_7O$ [M]$^+$; found, 577.69 [M] $^+$.

3.1.26. (4-(5-Benzylpyrimidin-2-yl)piperazin-1-yl)(4-((2-phenylquinazolin-4-ylamino)methyl)phenyl)methanone (**24**)

Compound **24** was prepared from intermediate **2** (120 mg, 0.472 mmol) and intermediate **12** (167 mg, 0.472 mmol) following the same procedure utilized in the preparation of **13**. The product obtained was a white solid (59 mg, 10%); mp: 216–217 °C. The purity of **24** was confirmed using HPLC (97.27%, R_t = 19.543). ^{1}H NMR (DMSO-*d6*): δ 3.37–3.79 (br, m, 10H), 4.99 (d, *J* = 5.82 Hz, 2H), 7.19–7.31 (m, 5H), 7.42–7.66 (m, 8H), 7.82 (m, 2H), 8.3 (s, 2H), 8.35

(d, $J = 8.22$ Hz, 1H), 8.44–8.47 (m, 2H), 9.02 (t, $J = 5.82$ Hz, 1H). ^{13}C NMR (DMSO-*d6*): δ 34.51, 43.24, 43.56, 113.79, 122.68, 122.88, 125.45, 126.1, 127.23, 127.3, 127.84, 128.2, 128.31, 128.53, 130.04, 132.83, 134.24, 138.52, 140.83, 141.51, 149.98, 157.77, 159.15, 159.58, 160.09, 169.12. MS: calcd 591.27 for $C_{37}H_{33}N_7O$ $[M]^+$; found, 591.69 $[M]^+$.

3.2. Antiproliferative cellular screening

3.2.1. MTT viability assay

MDA-MB-468 human breast cells were obtained from ATCC and cultured in RPMI 1640 medium (ATCC) supplemented with 10% FBS (Invitrogen), and 2% antibiotic-antimycotic mixture of Penicillin-G, Streptomycin sulfate, and Amphotericin B (Invitrogen) in a 5% CO_2 – 95% humidity incubator at 37 °C. 3-[4,5-dimethylthiazol-2-yl]-2,5-diphenyltetrazoliumbromide (MTT) assay was chosen to determine the IC_{50} (the concentration required to decrease cell viability by 50%) of the test compounds (**4**, **15**, and **16**) against the MDA-MB-468 cell line using gefitinib as a positive control [76]. 5000 cells, in 100 uL of the culture medium, were plated per well in 96-well plates. Cells were allowed to adhere for 1 day. Cells were then treated with fresh culture medium containing one of several concentrations of the test compounds; 100, 10, 1, 0.1, 0.01, 0.001 μM (final DMSO concentration was 1% irrelevant to the test compounds' concentration). The plates were processed after 48, 72, or 120 h via discarding the media and adding 100 uL 0.5 mg/ml MTT reagent in fresh culture media. The plates were then incubated for 4 h under 10% CO2 at 37 °C. The media was then removed and 100 uL of DMSO was added to each well to dissolve the formed formazone crystals. Plates were kept at room temperature over night away from light. The optical density of the formed violet color was quantified using an automatic spectrophotometer (Tristar LB 941) at a wavelength of 562 nm. The experiment was carried out with triplicate for each concentration of a given compound. Three independent experiments were conducted on three different dates. The concentration required for 50% reduction in the optical density, and hence the viability compared to control vehicle treated wells, was estimated for each compound against the studied cell line by non-linear regression analysis of the Log_{10} concentration in moles versus % viability curves. Curve fitting was performed using the variable slope-four parameter module implemented in the GraphPad Prism software (version 5.02).

3.2.2. Growth inhibition against NCI-60 panel

The SRB (sulforhodamine B) assay was used to measure the ability of a test compound to inhibit the growth of a given cell line [31]. The cell lines used in the NCI-60 are maintained using RPMI 1640 medium supplemented with 5% fetal bovine serum and 2 mM L-glutamine. Cell lines are seeded into a series of 96-well microtiter plates, with varied inoculation densities, depending on the growth rate and doubling time of each cell line. The plates are then incubated at 37 °C, 5 % CO_2, 95 % air and 100 % relative humidity for 24 h before treating with the test compounds. On the treatment day, experimental agents are added to the cells with a series of target final concentrations: 100, 10, 1, 0.1, and 0.01 μM (final DMSO concentration was 0.25% irrelevant of the test compound's concentration). After 48 h treatments while being incubated under the above conditions, the cells are fixed with trichloroacetic acid (concentration differs according to the nature of the cell line; adherent or suspension) for one hour at 4 °C. After removal of the supernatant, the plates are washed with water several times and dried completely in the air. Then 100 μL of 0.4% sulforhodamine B (SRB) solution in 1% acetic acid is added for 10 min. The unbound dye is removed and the plates are washed with 1% acetic acid. The bound dye is then solubilized with 10 mM trizma base, and the absorbance is measured using a plate reader at 515 nm. The same treatment and measurement were performed for cells prior to treatment and were assigned T_Z (T-zero). The % growth was calculated using the following equation: growth $= (T_i - T_z) \times 100/(C - T_z)$, where T_i is the reading for the treated well after two days of the treatment with a certain concentration of a specific compound. C is the average reading measured in the untreated wells after two days of treatment with the vehicle. T_Z is the average reading measured prior to treatment. GI_{50} is the dose that causes 50% inhibition of the growth after the treatment time compared to the T_Z and calculated from $-50 = (T_i - T_z) \times 100/(C - T_z)$. TGI is the dose that causes a total inhibition of the growth and can be computed using the equation: $T_i = T_Z$. LC_{50} is the dose that kills 50% of the cells compared to the cell density at the treatment time and calculated from $-50 = (T_i - T_z) \times 100/T_z$. This experiment was performed by the National Cancer Institute (NCI).

3.3. Kinase targeting investigation

3.3.1. Kinase binding screening

Biotinylated kinase ligand was immobilized onto streptavidin coated magnetic beads and washed with blocking buffer. The beads were then incubated with DNA-tagged kinase in the presence of test compound for 1 h at room temperature. Binding reactions were carried out in 20% Seablock, 0.17 × PBS, 0.005% Tween 20, 6 mM DTT, in a final volume of 0.04 mL. Beads were then washed with wash buffer (PBS, 0.05% Tween 20), and then incubated with elution buffer (PBS, 0.05% Tween 20, 0.5 M non-biotinylated kinase ligand) and eluted. The kinase concentration in the eluate was then measured by quantitative PCR. The detected signal is proportional to the number of eluted DNA-tagged kinase molecules and hence to the binding potency of a given test compound. The results of this single dose screening are reported in the form of binding percentage of control (B-POC) which is defined as follows: $B - POC = [(\text{test compound signal} - \text{positive control signal}) \times 100]/(\text{negative control signal} - \text{positive control signal})$. The negative control signal is obtained by the vehicle and corresponds to B-POC = 100 %. The positive signal control is detected by a binding positive compound and its B-POC is 0%. The B-POC results are the average of duplicate measurements. The pictures showing interaction with the kinome were generated using the TREEspot data visualization (Fig. S1). In order to determine the K_d, the above procedure is followed at 11-point three fold serial dilution of the test compound, from 30 μM to 0.508 nM, with the result of a standard dose-response curve. The K_d is then calculated according to the following equation: $\text{response} = \text{background} + \text{signal} - \text{background}/1 + K_d^{\text{hill slope}} + \text{dose}^{\text{hill slope}}$, $\text{hill slope} = -1$.

During the K_d calculation, the final DMSO % was fixed at 2.5% regardless of the test compound concentration [35].

A non-linear least square fit with the Levenberg–Marquardt algorithm was implemented to fit the curves (Fig. S2). Kinase binding assays were performed by Ambit Bioscience (San Diego, CA, USA).

3.3.2. Functional kinase inhibition assay

This experiment was conducted by mixing the test kinase, 10 μM γ-^{33}P-ATP, positively charged substrate, magnesium acetate, 1 μM test compound, and reaction buffer at room temperature. The reaction is then stopped by the addition of phosphoric acid solution. 10 μL of the reaction is filtered through a P30 filament, washed properly, dried, and finally subjected to scintillation counting [45]. DMSO was used as a vehicle for test compounds and its concentration was 2% regardless of the serial dilution of tested agents. The inhibition of a given kinase is represented by the function percentage of control (F-POC) which is calculated as follows: $F - POC = [\text{mean}(\text{counts} - \text{blanks})]_{\text{test}} \times 100/[\text{mean}(\text{counts} -$

blanks)]$_{\text{negative control}}$. The assay was performed in duplicates. Dose-response curves were fitted using non-linear regression implemented in GraphPad Prism software (version 5.02). A Sigmoidal dose-response (variable slope) was used in this case (Fig. S3). Kinase inhibition assays were performed by Millipore Corp. (Dundee, UK).

3.4. Molecular docking

Autodock 4.0 software was used to predict the mode of binding of **4**, **15**, and 1**6** to the CSNK1D x-ray crystal structure, 1CKI, deposited in RCSB [68]. The coordinates of the central grid pint of the maps was $X = 48.655$, $Y = 3.886$, and $Z = 82.118$ while the three dimensions of the grid box was set to be 70 points with each point equivalent to 0.375 Å. Affinity grids were calculated for all the atom types of the ligands. The Lamarckian genetic algorithm was chosen to perform conformational searching using the default parameters except for parameter of ga_run which was set to 150. In case of compound **4**, the type-I binding mode wasn't predicted in the top ranked energy cluster, however, it was predicted among the second ranked energy cluster. For both **15** and **16**, the top ranked energy cluster was found to assume type-I binding mode. Those conformers who adopt type-I in each case are presented as in Fig. 4.

Acknowledgments

We thank the National Science Foundation for an NMR instrumentation grant (NSF-MRI-0722654), the National Cancer Institute, the University of the Pacific Faculty Research Committee for a Holmok Cancer Research Grant and Eberhardt Research Fellowship (WAR), and Dr. Phillip R. Oppenheimer, the Dean of the Thomas J. Long School of Pharmacy, for generously supporting this research.

Appendix. Supplementary data

Supplementary data associated with the article can be found in online version, at doi:10.1016/j.ejmech.2011.02.057.

References

[1] R.M. Eglen, T. Reisine, Assay and Drug Development Technologies 7 (2009) 22–43.
[2] R.M. Eglen, T. Reisine, Expert Opinion on Drug Discovery 5 (2010) 277–290.
[3] K. Parikh, M.P. Peppelenbosch, Cancer Research 70 (2010) 2575–2578.
[4] U. McDermott, J. Settleman, Journal of Clinical Oncology 27 (2009) 5650–5659.
[5] N.I.O.H, U.S. Department of Health and Human Services, Targeted Cancer Therapies (2010).http://www.cancer.gov/cancertopics/factsheet/Therapy/targeted.
[6] E. Selzer, Expert Review of Clinical Pharmacology 3 (2010) 161–163.
[7] I. Akritopoulou-Zanze, P.J. Hajduk, Drug Discovery Today 14 (2009) 291–297.
[8] M.A. Bogoyevitch, D.P. Fairlie, Drug Discovery Today 12 (2007) 622–633.
[9] D. Huang, T. Zhou, K. Lafleur, C. Nevado, A. Bioinformatics 26 (2009) 198–204.
[10] L.O. Kirkland, C. McInnes, Biochemical Pharmacology 77 (2009) 1561–1571.
[11] L.A. Smyth, I. Collins, Journal of Chemical Biology 2 (2009) 131–151.
[12] A.M. Aronov, B. McClain, C.S. Moody, M.A. Murcko, Journal of Medicinal Chemistry 51 (2008) 1214–1222.
[13] Z.A. Knight, K.M. Shokat, Chemistry and Biology 12 (2005) 621–637.
[14] R. Morphy, Journal of Medicinal Chemistry 53 (2010) 1413–1437.
[15] M.W. Karaman, S. Herrgard, D.K. Treiber, P. Gallant, C.E. Atteridge, B.T. Campbell, K.W. Chan, P. Ciceri, M.I. Davis, P.T. Edeen, R. Faraoni, M. Floyd, J.P. Hunt, D.J. Lockhart, Z.V. Milanov, M.J. Morrison, G. Pallares, H.K. Patel, S. Pritchard, L.M. Wodicka, P.P. Zarrinkar, Nature Biotechnology 26 (2008) 127–132.
[16] K.S. Gajiwaia, J.C. Wu, J. Christensen, G.D. Deshmukh, W. Diehl, J.P. Dinitto, J.M. English, M.J. Greig, Y.A. He, S.L. Jacques, E.A. Lunney, M. McTigue, D. Molina, T. Quenzer, P.A. Wells, X. Yu, Y. Zhang, A. Zou, M.R. Emmett, A.G. Marshall, H.M. Zhang, G.D. Demetri, Proceedings of the National Academy of Sciences of the United States of America 106 (2009) 1542–1547.
[17] E.R. Wood, A.T. Truesdale, O.B. McDonald, D. Yuan, A. Hassell, S.H. Dickerson, B. Ellis, C. Pennisi, E. Horne, K. Lackey, K.J. Alligood, D.W. Rusnak, T.M. Gilmer, L. Shewchuk, Cancer Research 64 (2004) 6652–6659.
[18] Y. Liu, N.S. Gray, Nature Chemical Biology 2 (2006) 358–364.
[19] B.S. Pan, G.K.Y. Chan, M. Chenard, A. Chi, L.J. Davis, S.V. Deshmukh, J.B. Gibbs, S. Gil, G. Hang, H. Hatch, J.P. Jewell, I. Kariv, J.D. Katz, K. Kunii, W. Lu, B.A. Lutterbach, C.P. Paweletz, X. Qu, J.F. Reilly, A.A. Szewczak, Q. Zeng, N.E. Kohl, C.J. Dinsmore, Cancer Research 70 (2010) 1524–1533.
[20] A. Petrelli, S. Giordano, Current Medicinal Chemistry 15 (2008) 422–432.
[21] S.L. McGovern, B.K. Shoichet, Journal of Medicinal Chemistry 46 (2003) 1478–1483.
[22] O. Fedorov, B. Marsden, V. Pogacic, P. Rellos, S. Müller, A.N. Bullock, J. Schwaller, M. Sundström, S. Knapp, Proceedings of the National Academy of Sciences of the United States of America 104 (2007) 20523–20528.
[23] H. Ma, S. Deacon, K. Horiuchi, Expert Opinion on Drug Discovery 3 (2008) 607–621.
[24] P. Bamborough, D. Drewry, G. Harper, G.K. Smith, K. Schneider, Journal of Medicinal Chemistry 51 (2008) 7898–7914.
[25] S.L. Kinnings, R.M. Jackson, Journal of Chemical Information and Modeling 49 (2009) 318–329.
[26] T. Christoffersen, T.K. Guren, K.L.G. Spindler, O. Dahl, P.E. Lønning, B.T. Gjertsen, European Journal of Pharmacology 625 (2009) 6–22.
[27] A.P. Martin, C. Mitchell, M. Rahmani, K.P. Nephew, S. Grant, P. Dent, Cancer Biology and Therapy 8 (2010) 2084–2096.
[28] G. Pags, R. Grépin, Journal of Oncology 2010 (2010) 1–8.
[29] C. Betschart, K. Hayakawa, O. Irie, J. Sakaki, G. Iwasaki, R. Lattmann, M. Missbach, N. Teno. USPTO, 2005/0054851A1, p. 35.
[30] R.H. Shoemaker, Nature Reviews Cancer 6 (2006) 813–823.
[31] P. Skehan, R. Storeng, D. Scudiero, A. Monks, J. McMahon, D. Vistica, J.T. Warren, H. Bokesch, S. Kenney, M.R. Boyd, Journal of the National Cancer Institute 82 (1990) 1107–1112.
[32] C.H. Takimoto, Cancer Chemotherapy and Pharmacology 52 (Suppl.) (2003) 29–33.
[33] C. Oliveras-Ferraros, A. Vazquez-Martin, E. López-Bonet, B. Martín-Castillo, S. Del Barco, J. Brunet, J.A. Menendez, International Journal of Oncology 33 (2008) 1165–1176.
[34] J. Nautiyal, Y. Yu, A. Aboukameel, S.S. Kanwar, J.K. Das, J. Du, B.B. Patel, F.H. Sarkar, A.K. Rishi, R.M. Mohammad, A.P.N. Majumdar, Molecular Cancer Therapeutics 9 (2010) 1503–1514.
[35] M.A. Fabian, W.H. Biggs Iii, D.K. Treiber, C.E. Atteridge, M.D. Azimioara, M.G. Benedetti, T.A. Carter, P. Ciceri, P.T. Edeen, M. Floyd, J.M. Ford, M. Galvin, J.L. Gerlach, R.M. Grotzfeld, S. Herrgard, D.E. Insko, M.A. Insko, A.G. Lai, J.M. Lélias, S.A. Mehta, Z.V. Milanov, A.M. Velasco, L.M. Wodicka, H.K. Patel, P.P. Zarrinkar, D.J. Lockhart, Nature Biotechnology 23 (2005) 329–336.
[36] L.H. Pettus, R.P. Wurz, S. Xu, B. Herberich, B. Henkle, Q. Liu, H.J. McBride, S. Mu, M.H. Plant, C.J.M. Saris, L. Sherman, L.M. Wong, S. Chmait, M.R. Lee, C. Mohr, F. Hsieh, A.S. Tasker, Journal of Medicinal Chemistry 53 (2010) 2973–2985.
[37] C.B. Andersen, Y. Wan, J.W. Chang, B. Riggs, C. Lee, Y. Liu, F. Sessa, F. Villa, N. Kwiatkowski, M. Suzuki, L. Nallan, R. Heald, A. Musacchio, N.S. Gray, ACS Chemical Biology 3 (2008) 180–192.
[38] J.K. Jiang, K. Ghoreschi, F. Deflorian, Z. Chen, M. Perreira, M. Pesu, J. Smith, D.T. Nguyen, E.H. Liu, W. Leister, S. Costanzi, J.J. O'Shea, C.J. Thomas, Journal of Medicinal Chemistry 51 (2008) 8012–8018.
[39] C.J. Burns, M.F. Harte, X. Bu, E. Fantino, M. Giarrusso, M. Joffe, M. Kurek, F.S. Legge, P. Razzino, S. Su, H. Treutlein, S.S. Wan, J. Zeng, A.F. Wilks, Bioorganic and Medicinal Chemistry Letters 19 (2009) 1206–1209.
[40] Q. Chao, K.G. Sprankle, R.M. Grotzfeld, A.G. Lai, T.A. Carter, A.M. Velasco, R.N. Gunawardane, M.D. Cramer, M.F. Gardner, J. James, P.P. Zarrinkar, H.K. Patel, S.S. Bhagwat, Journal of Medicinal Chemistry 52 (2009) 7808–7816.
[41] W.S. Yang, B.R. Stockwell, Genome Biology 9 (R92) (2008) 1–13.
[42] N. Oumata, K. Bettayeb, Y. Ferandin, L. Demange, A. Lopez-Giral, M.L. Goddard, V. Myrianthopoulos, E. Mikros, M. Flajolet, P. Greengard, L. Meijer, H. Galons, Journal of Medicinal Chemistry 51 (2008) 5229–5242.
[43] M.H. Cohen, G. Williams, J.R. Johnson, J. Duan, J. Gobburu, A. Rahman, K. Benson, J. Leighton, S.K. Kim, R. Wood, M. Rothmann, G. Chen, K.M. U, A.M. Staten, R. Pazdur, Clinical Cancer Research 8 (2002) 935–942.
[44] R. Dagher, M. Cohen, G. Williams, M. Rothmann, J. Gobburu, G. Robbie, A. Rahman, G. Chen, A. Staten, D. Griebel, R. Pazdur, Clinical Cancer Research 8 (2002) 3034–3038.
[45] S.P. Davies, H. Reddy, M. Caivano, P. Cohen, Biochemical Journal 351 (2000) 95–105.
[46] R.A. Copeland, Analytical Biochemistry 320 (2003) 1–12.
[47] M.C. Heinrich, C.L. Corless, A. Duensing, L. McGreevey, C.J. Chen, N. Joseph, S. Singer, D.J. Griffith, A. Haley, A. Town, G.D. Demetri, C.D.M. Fletcher, J.A. Fletcher, Science 299 (2003) 708–710.
[48] K. Masson, L. Ronnstrand, Cellular Signalling 21 (2009) 1717–1726.
[49] H. Bougherara, F. Subra, R. Crepin, P. Tauc, C. Auclair, M.A. Poul, Molecular Cancer Research 7 (2009) 1525–1533.
[50] B. Liegl-Atzwanger, J.A. Fletcher, C.D.M. Fletcher, Virchows Archiv 456 (2010) 111–127.
[51] B. Pasini, L. Matyakhina, T. Bei, M. Muchow, S. Boikos, B. Ferrando, J.A. Carney, C.A. Stratakis, Journal of Clinical Endocrinology and Metabolism 92 (2007) 3728–3732.
[52] E. Weisberg, R.D. Wright, J. Jiang, A. Ray, D. Moreno, P.W. Manley, D. Fabbro, E. Hall-Meyers, L. Catley, K. Podar, A.L. Kung, J.D. Griffin, Gastroenterology 131 (2006) 1734–1742.
[53] B.M.J.M. Suijkerbuijk, I. Niculescu-Duvaz, C. Gaulon, H.P. Dijkstra, D. Niculescu-Duvaz, D. Ménard, A. Zambon, A. Nourry, L. Davies, H.A. Manne, F. Friedlos, L.M. Ogilvie, D. Hedley, F. Lopes, N.P.U. Preece, J. Moreno-Farre,

F.I. Raynaud, R. Kirk, S. Whittaker, R. Marais, C.J. Springer, Journal of Medicinal Chemistry 53 (2010) 2741–2756.
[54] E. Jabbour, H.M. Kantarjian, D. Jones, N. Reddy, S. O'Brien, G. Garcia-Manero, J. Burger, J. Cortes, Blood 112 (2008) 4839–4842.
[55] D.G. Aguilera, A.M. Tsimberidou, Therapeutics and Clinical Risk Management 5 (2009) 281–289.
[56] S. Branford, J.V. Melo, T.P. Hughes, Blood 114 (2009) 5426–5435.
[57] P. Kolb, D. Huang, F. Dey, A. Caflisch, Journal of Medicinal Chemistry 51 (2008) 1179–1188.
[58] M.D.M. AbdulHameed, A. Hamza, C.G. Zhan, Journal of Physical Chemistry B 110 (2006) 26365–26374.
[59] O. Rixe, S.X. Franco, D.A. Yardley, S.R. Johnston, M. Martin, B.K. Arun, S.P. Letrent, H.S. Rugo, Cancer Chemotherapy and Pharmacology 64 (2009) 1139–1148.
[60] E. Weisberg, J. Roesel, G. Bold, P. Furet, J. Jiang, J. Cools, R.D. Wright, E. Nelson, R. Barrett, A. Ray, D. Moreno, E. Hall-Meyers, R. Stone, I. Galinsky, E. Fox, G. Gilliland, J.F. Daley, S. Lazo-Kallanian, A.L. Kung, J.D. Griffin, Blood 112 (2008) 5161–5170.
[61] S. Baumli, G. Lolli, E.D. Lowe, S. Troiani, L. Rusconi, A.N. Bullock, J.E. Debreczeni, S. Knapp, L.N. Johnson, EMBO Journal 27 (2008) 1907–1918.
[62] C.H. Yun, T.J. Boggon, Y. Li, M.S. Woo, H. Greulich, M. Meyerson, M.J. Eck, Cancer Cell 11 (2007) 217–227.
[63] T.J. Boggon, Y. Li, P.W. Manley, M.J. Eck, Blood 106 (2005) 996–1002.
[64] J. Stamos, M.X. Sliwkowski, C. Eigenbrot, Journal of Biological Chemistry 277 (2002) 46265–46272.
[65] M. Torrent, K. Rickert, B.S. Pan, L. Sepp-Lorenzino, Journal of Molecular Graphics and Modelling 23 (2004) 153–165.
[66] R. Foster, R. Griffith, P. Ferrao, L. Ashman, Journal of Molecular Graphics and Modelling 23 (2004) 139–152.
[67] G. Morris, R. Huey, W. Lindstrom, M. Sanner, R. Belew, D.S. Goodsell, A. Olson, Journal of Computational Chemistry 30 (2009) 2785–2791.
[68] K. Longenecker, P. Roach, T. Hurley, Journal of Molecular Biology 257 (1996) 618–631.
[69] D. Goldfarb. USPTO, 2009/0163545A1, p.57.
[70] V.M. Sapelkin, A.G. Golub, O. Yakovenko, V.G. Bdzhola, S.M. Yarmoluk, Ukrainica Bioorganica Acta 1 (2004) 74–79.
[71] N.T. Solonskaya, V.I. Bliznyukov, Farmatsevtichnii Zhurnal 26 (1971) 21–25.
[72] V. Rahul, B. Kazimierz, B. Jean-Louis, N. Deogratias, W. Chang-Qing, Z. Robert Joseph. WO 2007/071055A1, p.155.
[73] S.J. Baker, S.M. Firestine, D. Smithrud, F. Salinas, S.J. Benkovic, Tetrahedron Letters 41 (2000) 7009–7012.
[74] V. Rahul, D. Gilles, W. Chang-Qing, G. Zhonghong, N. Deogratias, B. Jean-Louis, P. Michel, E. Aram. WO 2009/000085A1, p.152.
[75] H. Cope, R. Mutter, W. Heal, C. Pascoe, P. Brown, S. Pratt, B. Chen, European Journal of Medicinal Chemistry 41 (2006) 1124–1143.
[76] T. Mosmann, Journal of Immunological Methods 65 (1983) 55–63.